

In the format provided by the authors and unedited.

# Data-driven prediction of battery cycle life before capacity degradation

Kristen A. Severson <sup>1,5</sup>, Peter M. Attia  <sup>2,5</sup>, Norman Jin  <sup>2</sup>, Nicholas Perkins  <sup>2</sup>, Benben Jiang  <sup>1</sup>, Zi Yang  <sup>2</sup>, Michael H. Chen  <sup>2</sup>, Muratahan Aykol  <sup>3</sup>, Patrick K. Herring  <sup>3</sup>, Dimitrios Fraggedakis  <sup>1</sup>, Martin Z. Bazant  <sup>1</sup>, Stephen J. Harris  <sup>2,4</sup>, William C. Chueh  <sup>2\*</sup> and Richard D. Braatz  <sup>1\*</sup>

---

<sup>1</sup>Department of Chemical Engineering, Massachusetts Institute of Technology, Cambridge, MA, USA. <sup>2</sup>Department of Materials Science and Engineering, Stanford University, Stanford, CA, USA. <sup>3</sup>Toyota Research Institute, Los Altos, CA, USA. <sup>4</sup>Materials Science Division, Lawrence Berkeley National Lab, Berkeley, CA, USA. <sup>5</sup>These authors contributed equally: K. A. Severson, P. M. Attia. \*e-mail: [wchueh@stanford.edu](mailto:wchueh@stanford.edu); [braatz@mit.edu](mailto:braatz@mit.edu)

**Supplementary Information for**

**Data-driven prediction of battery cycle life before capacity degradation**

Kristen A. Severson<sup>1\*</sup>, Peter M. Attia<sup>2\*</sup>, Norman Jin<sup>2</sup>, Nicholas Perkins<sup>2</sup>, Benben Jiang<sup>1</sup>, Zi Yang<sup>2</sup>, Michael H. Chen<sup>2</sup>, Muratahan Aykol<sup>3</sup>, Patrick K. Herring<sup>3</sup>, Dimitrios Fraggedakis<sup>1</sup>, Martin Z. Bazant<sup>1</sup>, Stephen J. Harris<sup>4</sup>, William C. Chueh<sup>2†</sup>, Richard D. Braatz<sup>1†</sup>

\* These authors contributed equally to this work

† Corresponding authors: [wchueh@stanford.edu](mailto:wchueh@stanford.edu), [braatz@mit.edu](mailto:braatz@mit.edu)

**Affiliations:**

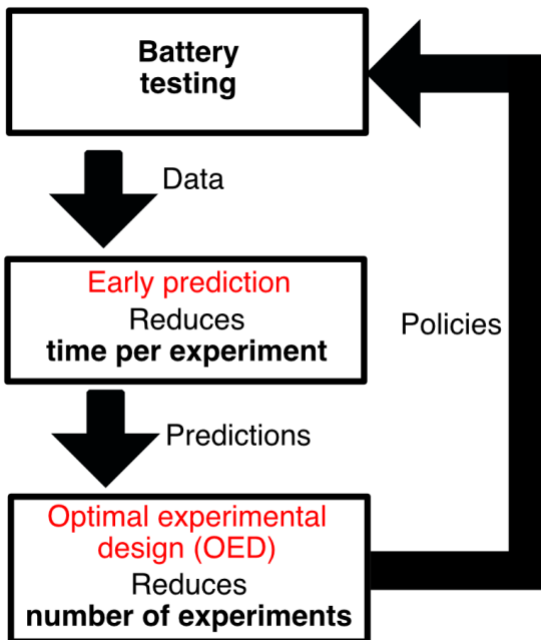
1 Department of Chemical Engineering, Massachusetts Institute of Technology, Cambridge, MA, USA

2 Department of Materials Science and Engineering, Stanford University, Stanford, CA, USA

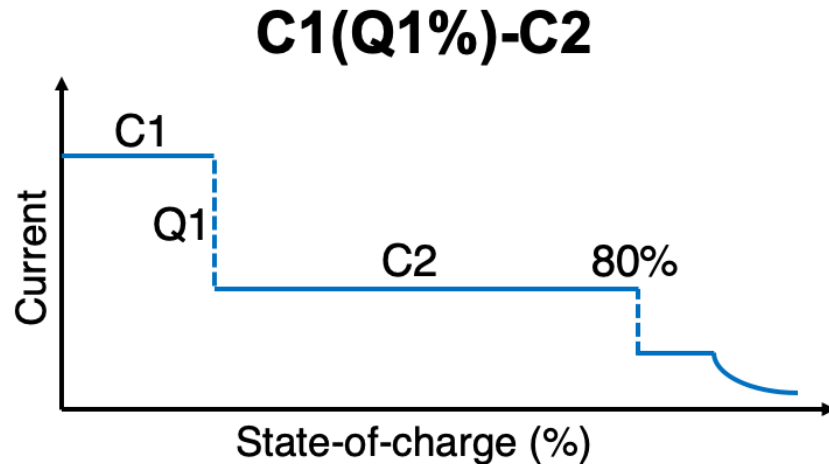
3 Toyota Research Institute, Los Altos, CA, USA

4 Materials Science Division, Lawrence Berkeley National Lab, Berkeley, CA, USA

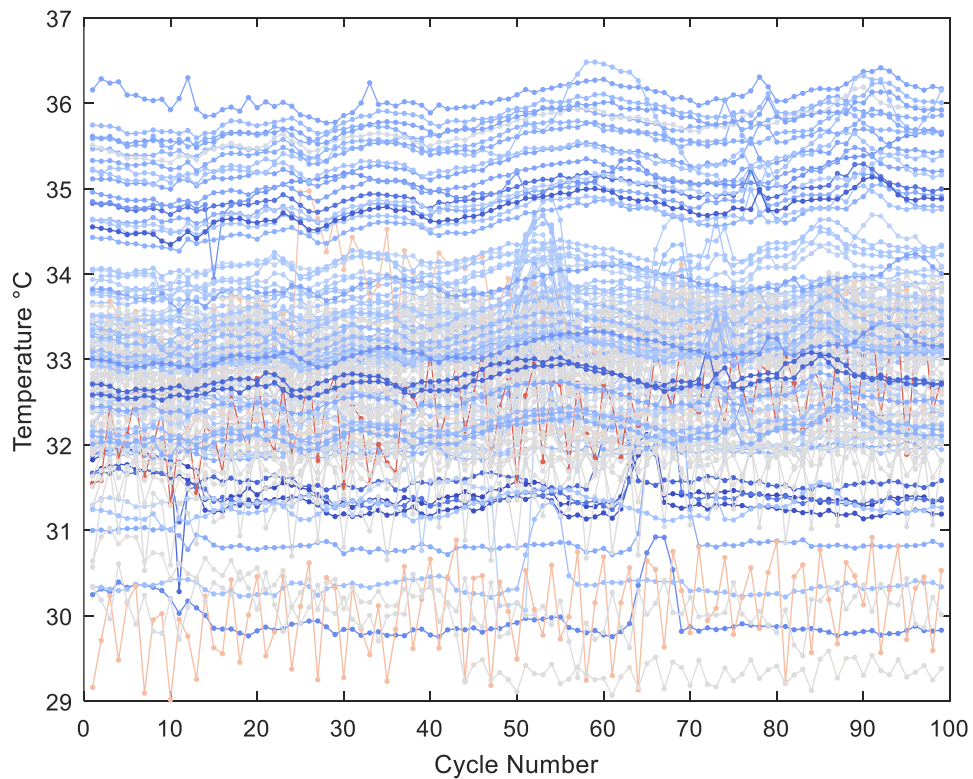
## Supplementary Figures



**Supplementary Figure 1.** Schematic illustrating a closed-loop optimization system. First, batteries are tested, and the data is inputted into an early prediction model. These predictions are subsequently inputted to a Bayesian optimal experimental design algorithm, which recommends the next policies to be tested. This process iterates until the testing budget is exhausted. With this approach, early prediction reduces the number of cycles required per tested cell, while optimal experimental design reduces the number of experiments required. This method can be applied to optimize battery chemistry, processing and management protocols, which often necessitates searching through a large parameter space and inevitably involves cycling many cells to failure. Early prediction of failure is a key component of high-throughput battery optimization applications.

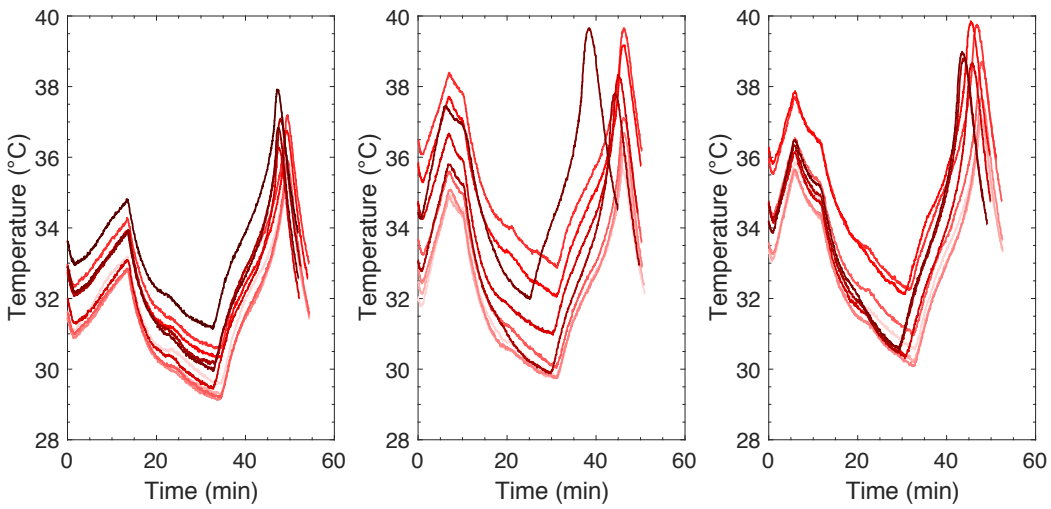


**Supplementary Figure 2.** Illustration of extreme fast charging policy structure (~10 minutes to 80% SOC). All cells in this dataset were tested with a two-step fast charging policy. C1 and C2 represent the first and second applied currents, while Q1 represents the SOC (%) at which the currents switch. Beyond 80% SOC, all cells charge galvanostatically at 1C to 3.6 V and then charge potentiostatically at 3.6 V. The upper value for each current is constrained by the manufacturer's upper voltage limit (3.6 V).

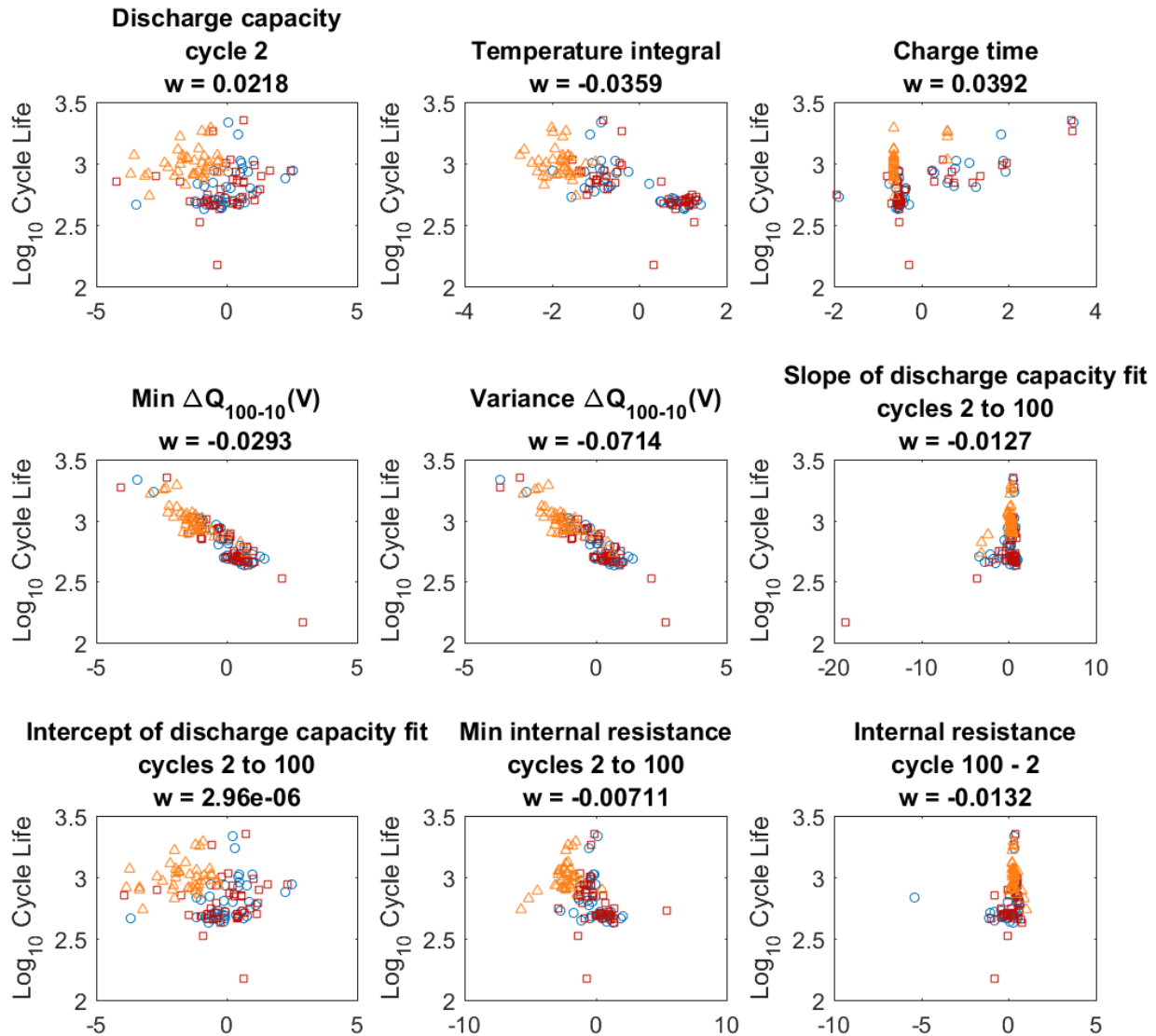


**Supplementary Figure 3.** Average cell temperature as a function of cycle number for all cells.

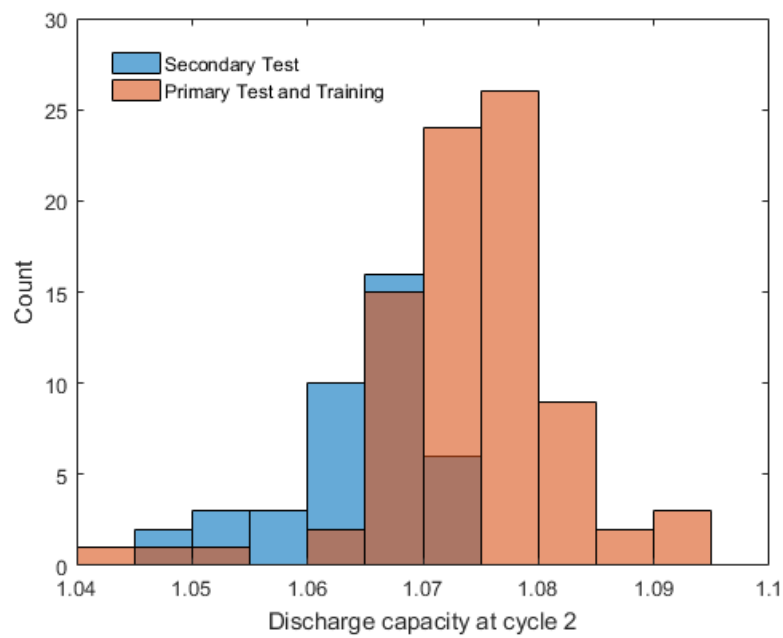
The color represents cycle life. The average temperature varies by around 6°C over all cells, largely as a function of charging policy, position within the temperature chamber, internal cell impedance, and batch.



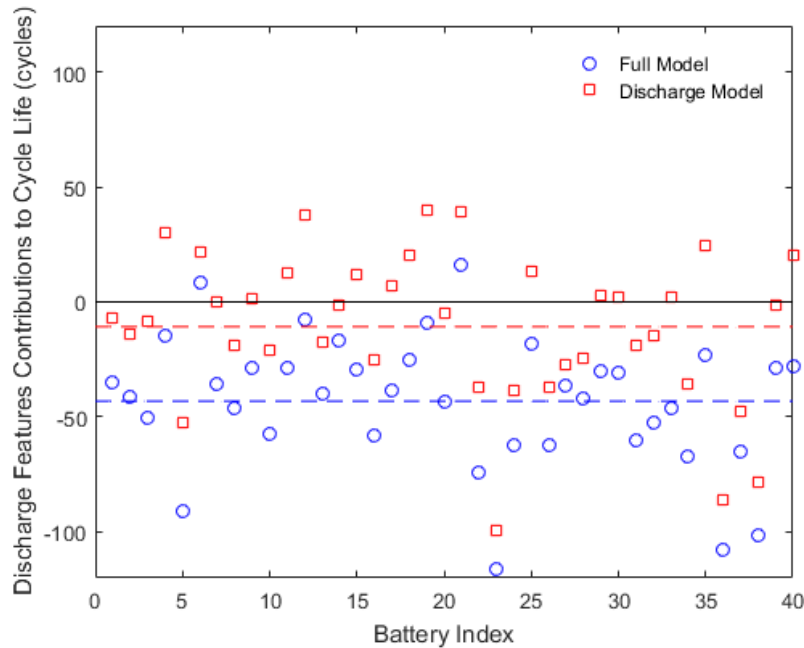
**Supplementary Figure 4.** Temperature profiles as a function of time and cycle number for three different cells. Each line represents a 100-cycle increment, and darker colors represent higher cycle number. The peak around 10 minutes is the peak during charge, which varies substantially as a function of charging policy, while the peak around 50 minutes is the peak during the 4C discharge. The temperature rises substantially during the rapid charge and discharge steps, in some cases increasing by nearly  $10^{\circ}\text{C}$ . The temperature profiles generally rise as a function of cycle number as the cell impedance increases. Note that the contact between the cell and the thermocouple may vary during cycling as well.



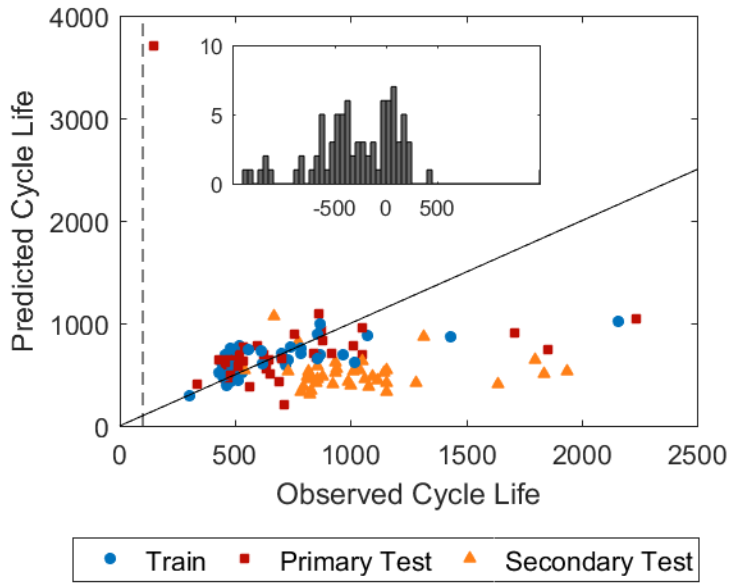
**Supplementary Figure 5.** Nine features used in the full model described in Supplementary Table 1. The coefficient value for the feature in the linear model is in the title of plot. The train, primary test, and secondary test cells are represented by blue circles, red squares, and orange triangles, respectively. The z-scored feature values are presented on the  $x$  axis. Z-scoring is performed based on the training data.



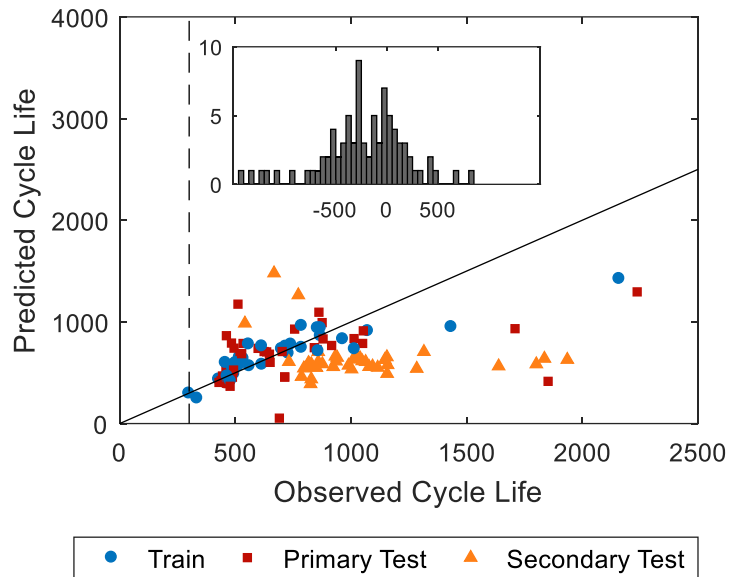
**Supplementary Figure 6.** Histogram of initial discharge capacity (cycle 2) for the secondary test dataset compared to the training and primary test datasets.



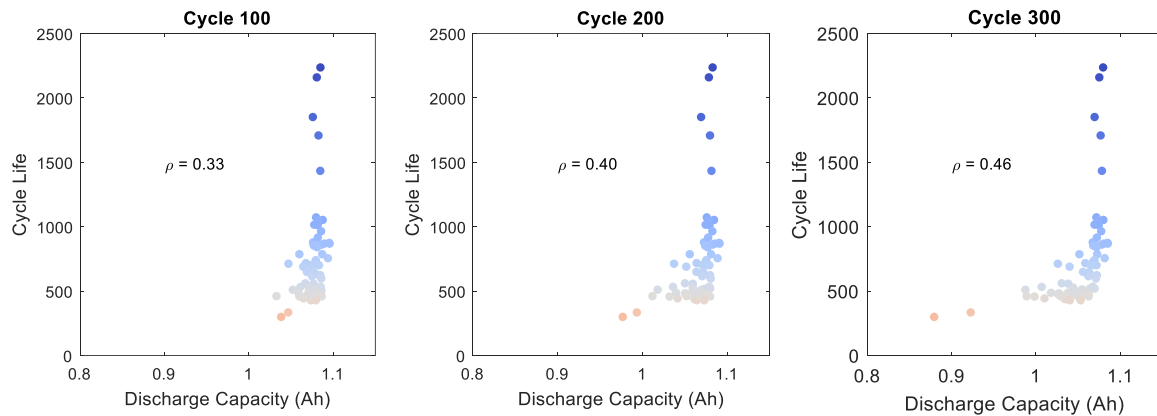
**Supplementary Figure 7.** Contributions from the discharge features to cycle life for the full model and the discharge model for the secondary test dataset as compared to the average prediction. The mean offset for the full and discharge models are given by the dotted lines. The discharge features may be biased in the full model due to the specific discharge features selected by the elastic net.



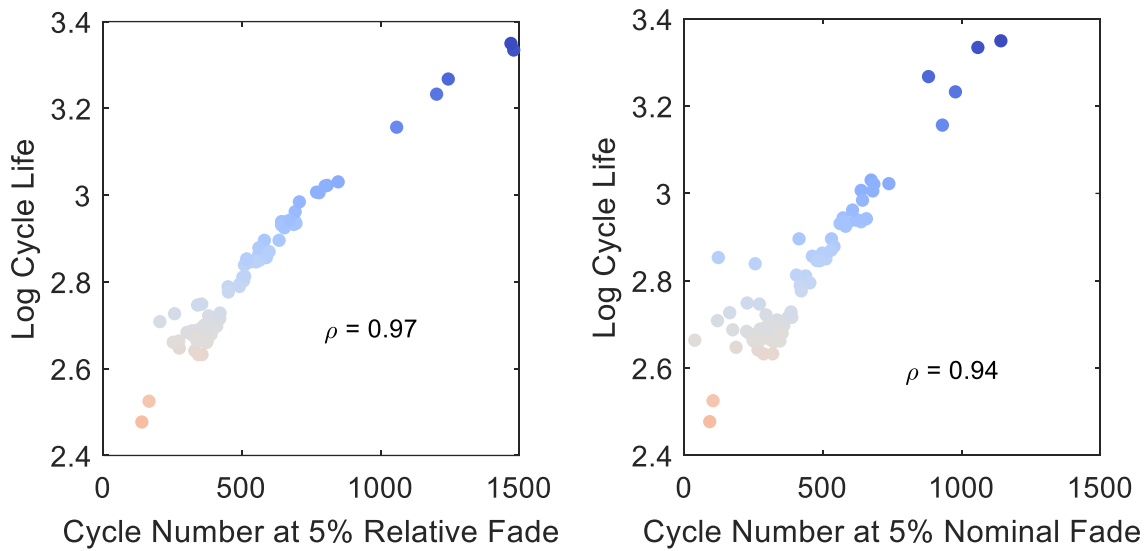
**Supplementary Figure 8.** Observed and predicted cycle lives for the “multivariate discharge curve, cycle 100” model. The training data are used to learn the model structure and coefficient values, and the testing data are used to assess the generalizability of the model. The vertical dotted line indicates when the prediction is made in relation to the observed cycle life. The features used in the model can be found in Supplementary Table 2. The inset shows the histogram of residuals (predicted – observed) for the primary and secondary test data; the residual for the outlier cell is not shown in the inset.



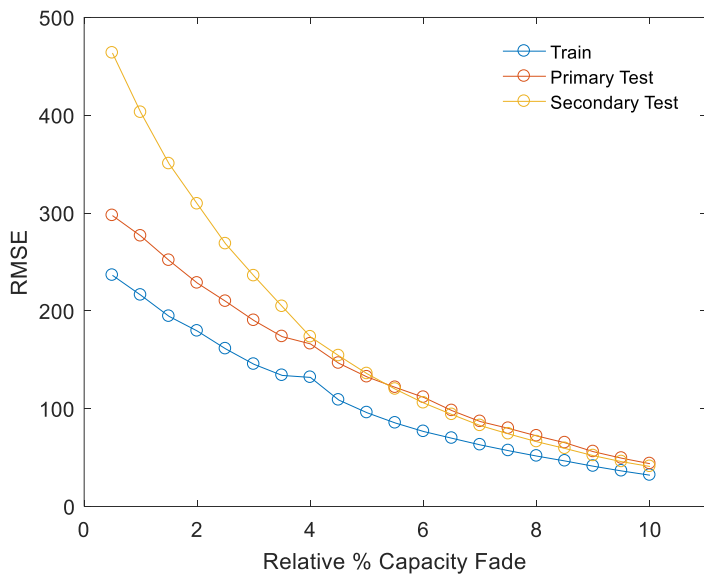
**Supplementary Figure 9.** Observed and predicted cycle lives for the “multivariate discharge curve, cycle 300” model. The training data are used to learn the model structure and coefficient values, and the testing data are used to assess the generalizability of the model. The vertical dotted line indicates when the prediction is made in relation to the observed cycle life. The features used in the model can be found in Supplementary Table 2. The inset shows the histogram of residuals (predicted – observed) for the primary and secondary test data. The outlier cell has a cycle life of 148 and is therefore not included in analysis.



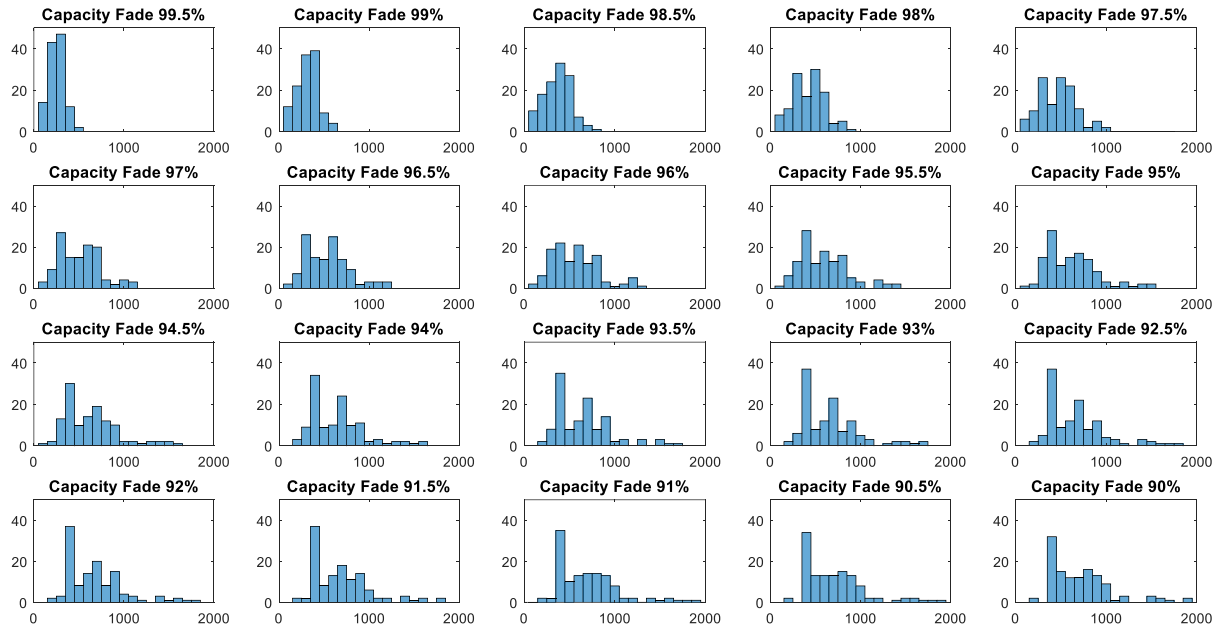
**Supplementary Figure 10.** Relationship between cycle life and the discharge capacity at cycles 100, 200, and 300. The correlation coefficient,  $\rho$ , is also displayed. The short-lived outlier cell is excluded from analysis.



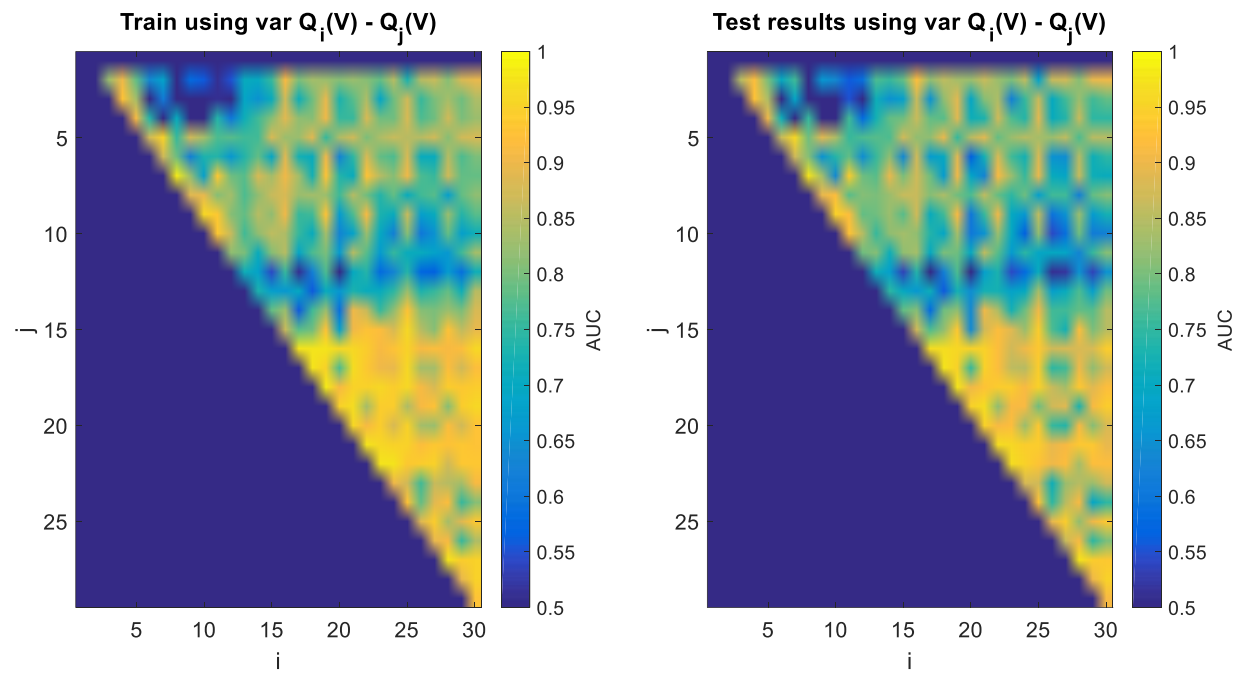
**Supplementary Figure 11.** Correlation between log cycle life and the number of cycles to reach 5% total capacity fade. Relative fade (left) is with respect to the observed discharge capacity at cycle 2, and absolute fade (right) is with respect to the nominal discharge capacity (1.1 Ah). The correlation coefficient,  $\rho$ , is also displayed.



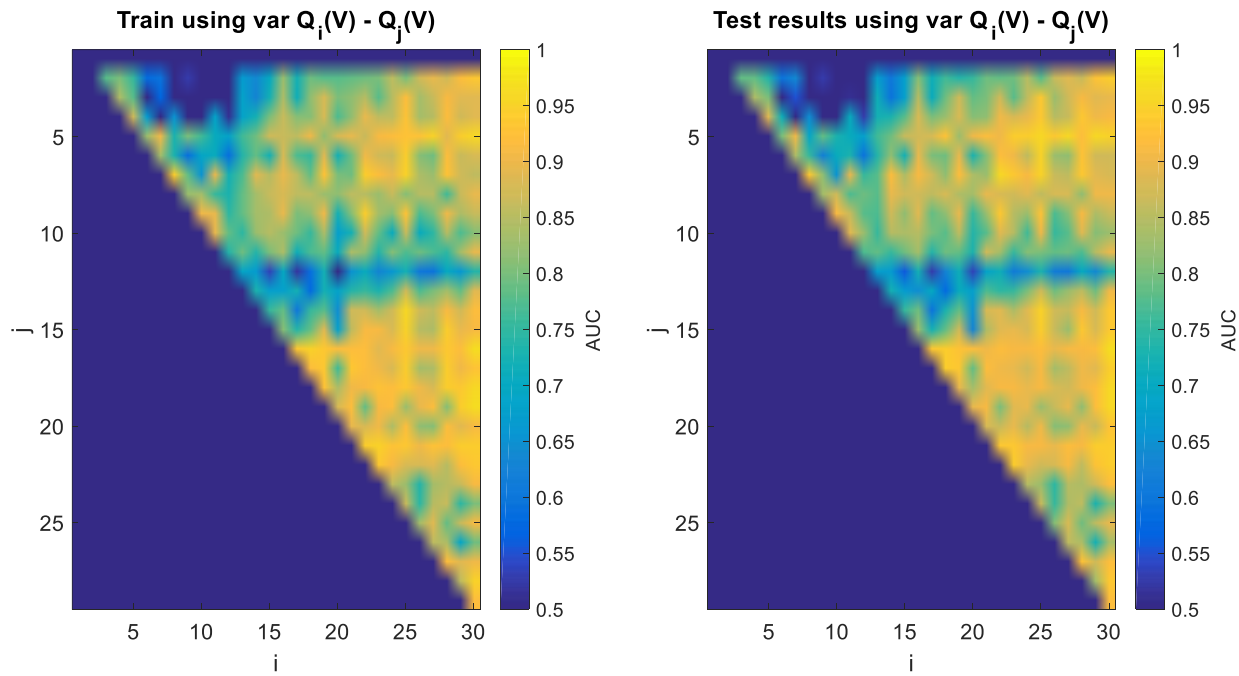
**Supplementary Figure 12.** The RMSE of models using the log cycle number at which the capacity fade criteria are met.



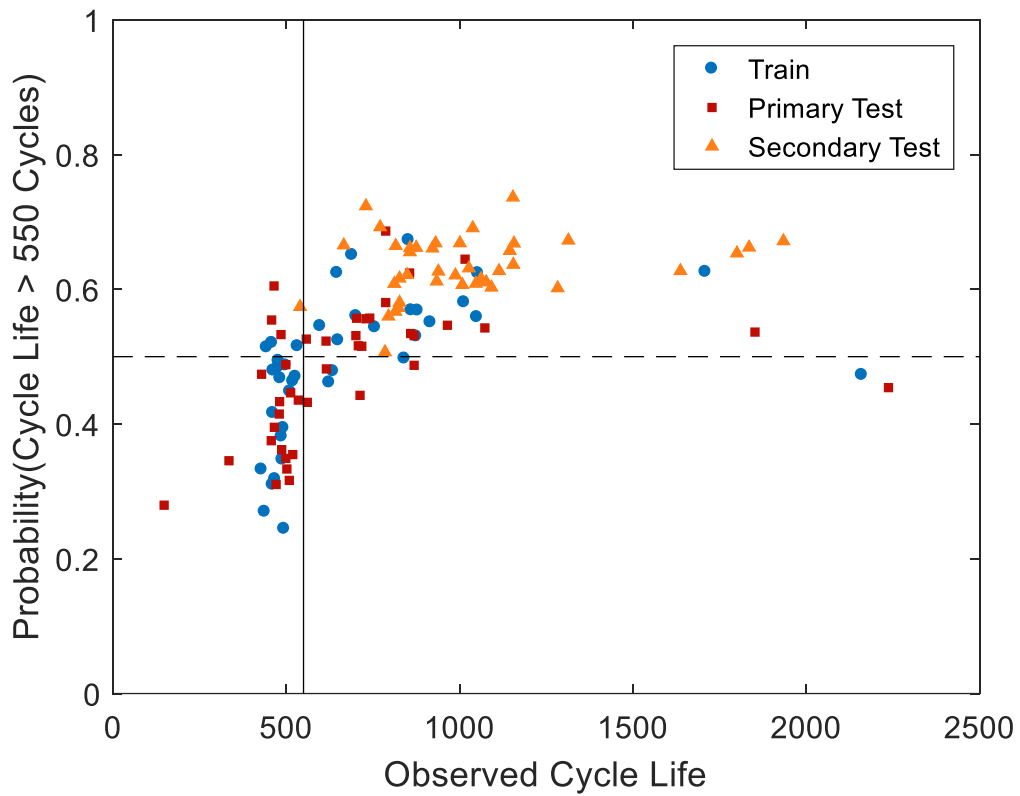
**Supplementary Figure 13.** Distribution of the cycle numbers at which predictions are made as a function of the capacity fade criterion.



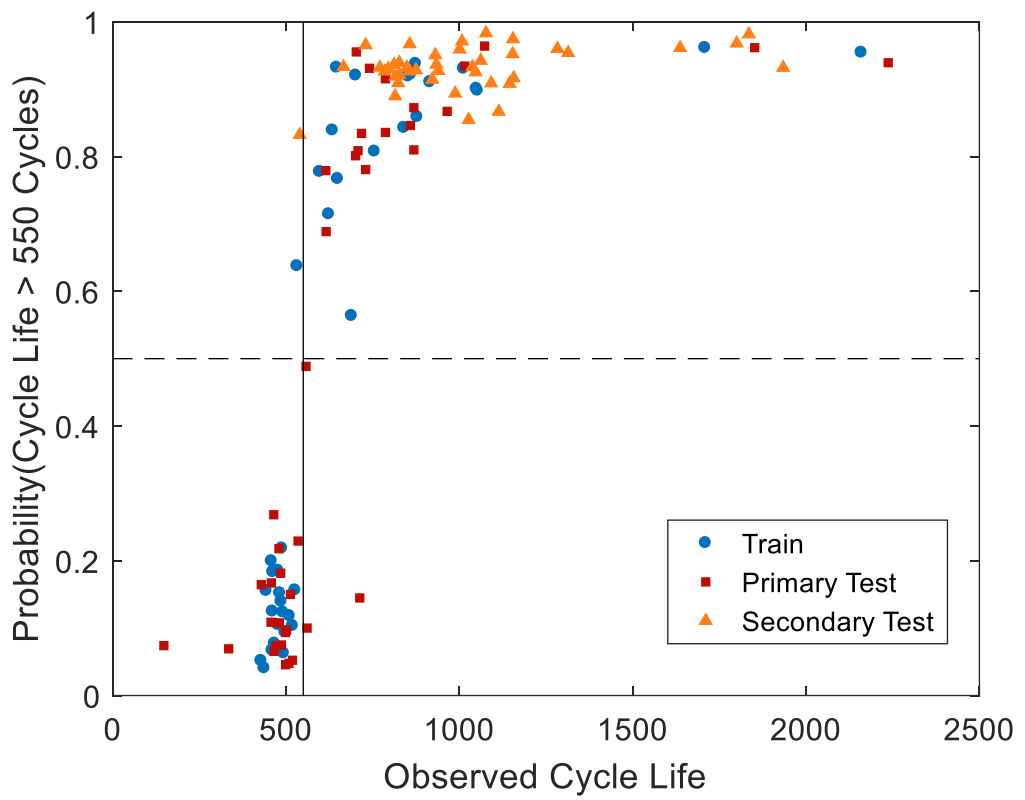
**Supplementary Figure 14.** Average AUC for 20 random train/test splits in the classification setting using a lifetime threshold of 550 cycles.



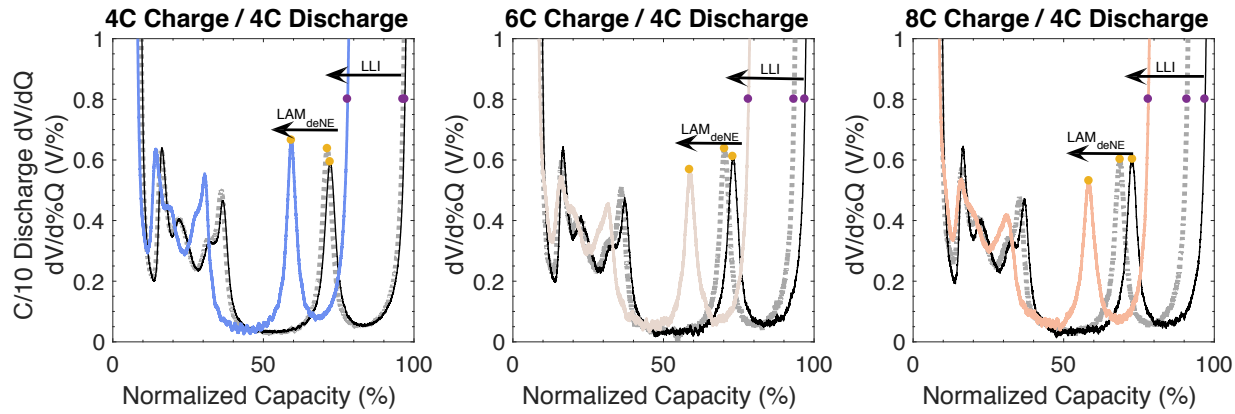
**Supplementary Figure 15.** Average AUC for 20 random train/test splits in the classification setting using a lifetime threshold of 700 cycles.



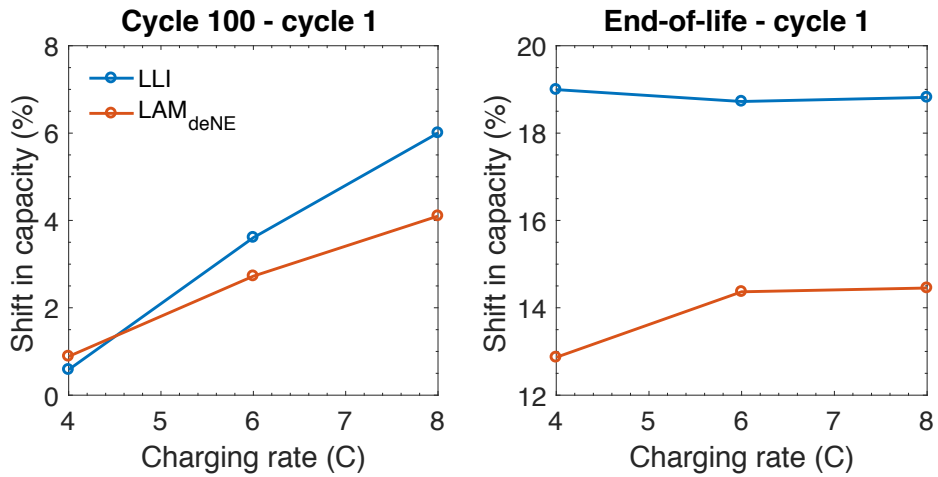
**Supplementary Figure 16.** The probability of a battery's lifetime exceeding the lifetime threshold of 550 cycles vs observed cycle life using the “variance classifier”. The decision boundary is 0.5. The variance of  $\Delta Q(V) = Q_5(V) - Q_4(V)$  is the only feature in this classification model.



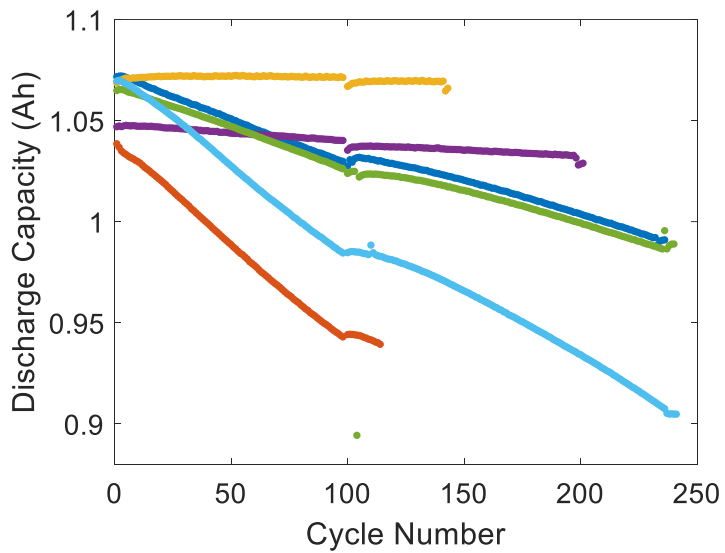
**Supplementary Figure 17.** The probability of a battery's lifetime exceeding the lifetime threshold of 550 cycles vs observed cycle life using the “full classifier”. The decision boundary is 0.5. Five cycles were used in this classification task.



**Supplementary Figure 18.** Identification of shifts in  $dV/dQ$  for loss of lithium inventory (LLI) and loss of active delithiated negative electrode material (LAM<sub>deNE</sub>). This figure is identical to the second row of Figure 4 but with additional annotations. As a measure of LLI, we use the change in normalized capacity at 0.8 V/% (purple dots). As a measure of LAM<sub>deNE</sub>, we use the shift in the peak position for the peak near 75% of normalized capacity (yellow dots).

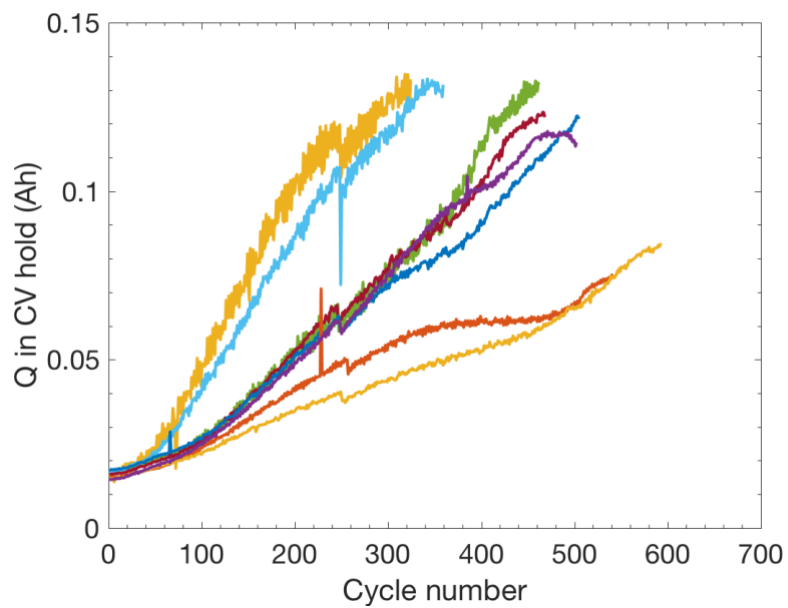


**Supplementary Figure 19.** Shifts for loss of lithium inventory (LLI) and loss of active delithiated negative electrode material ( $\text{LAM}_{\text{deNE}}$ ) as a function of C rate during charging (measured at 4C, 6C, and 8C). The left subplot displays the shift from cycle 1 to cycle 100. The right subplot displays the shift from cycle 1 to the end-of-life.

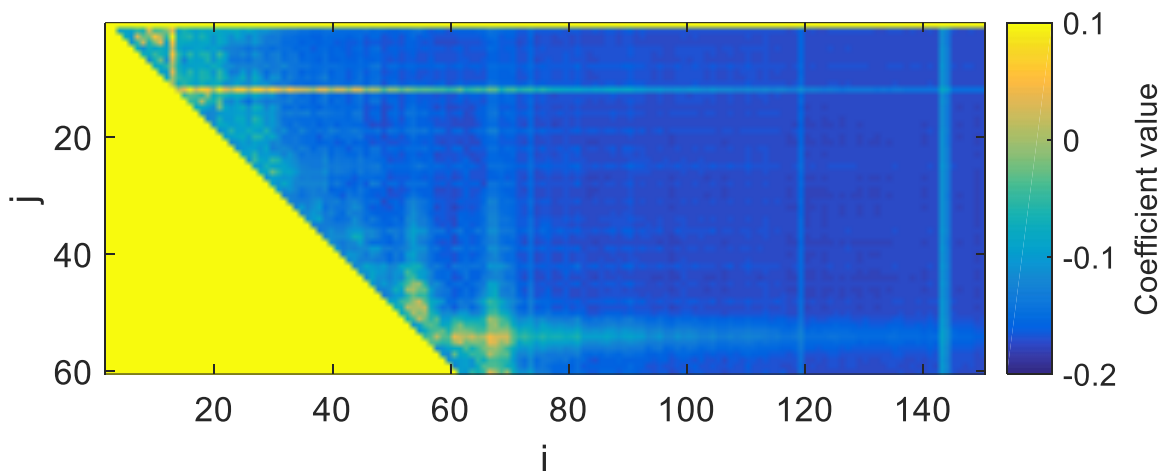


**Supplementary Figure 20.** Discharge capacity curves for batteries with periodic slow charging.

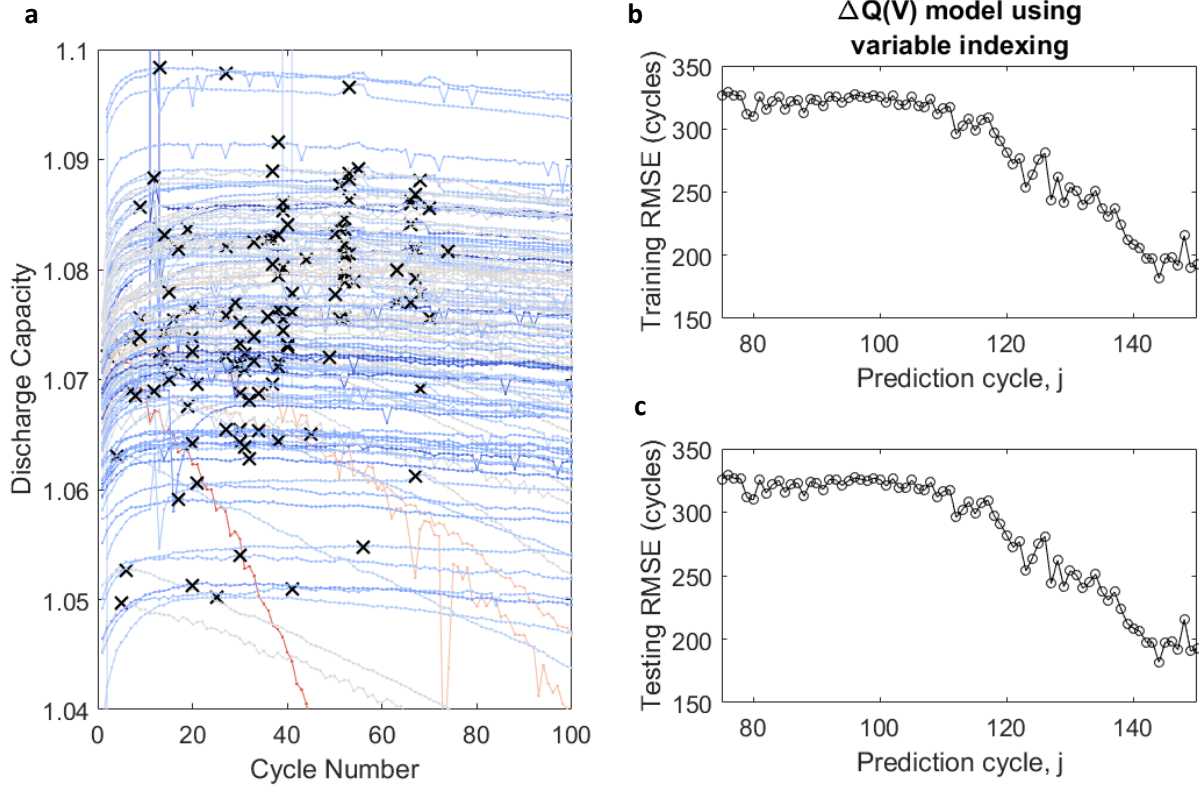
A slow (C/10) charge and discharge cycle is employed at cycle 100, often resulting in a brief increase in discharge capacity on subsequent cycles (particularly for highly-degrading cells).



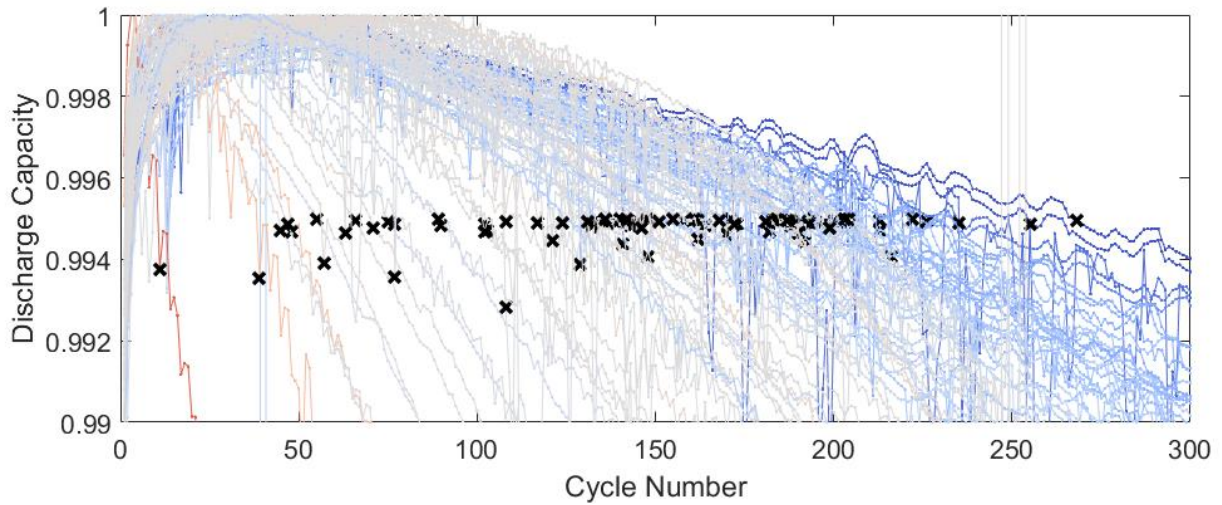
**Supplementary Figure 21.** Measured capacity during the constant-voltage hold at the end of discharge as a function of cycle number for four representative cells. The lower cutoff potential is 2 V, and the current cutoff condition is C/50 (0.022 A).



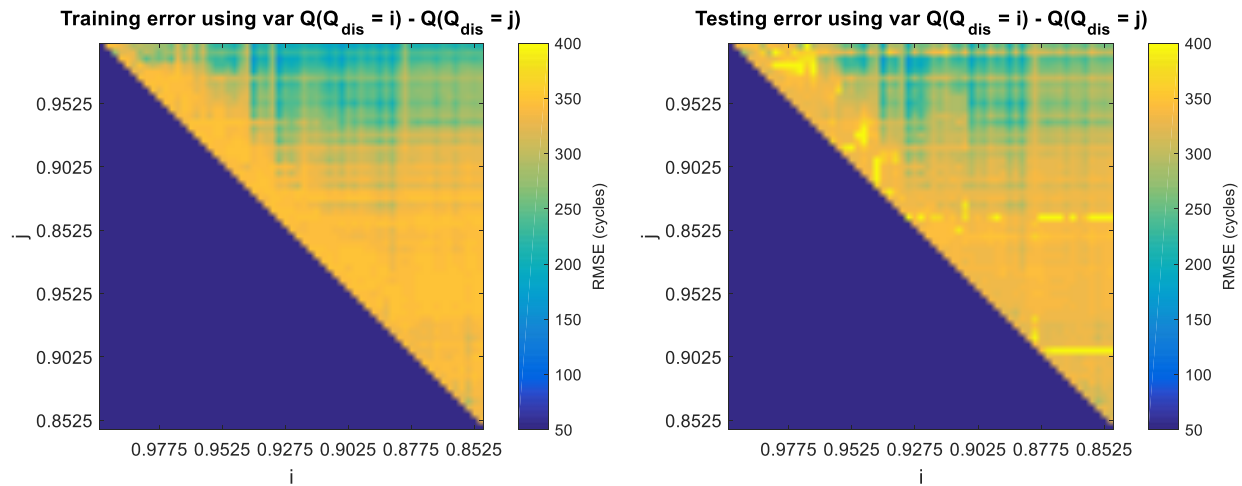
**Supplementary Figure 22.** Value of the coefficients as a function of cycle indices mapping to the  $\Delta Q(V)$  feature in Figure 5. The model is  $\hat{y}_k = wx_k + b$ , where  $\hat{y}_k$  is the predicted cycle life for battery  $k$ ,  $x_k$  is the  $\Delta Q(V)$  feature for battery  $k$ ,  $w$  is the coefficient, and  $b$  is an offset term.



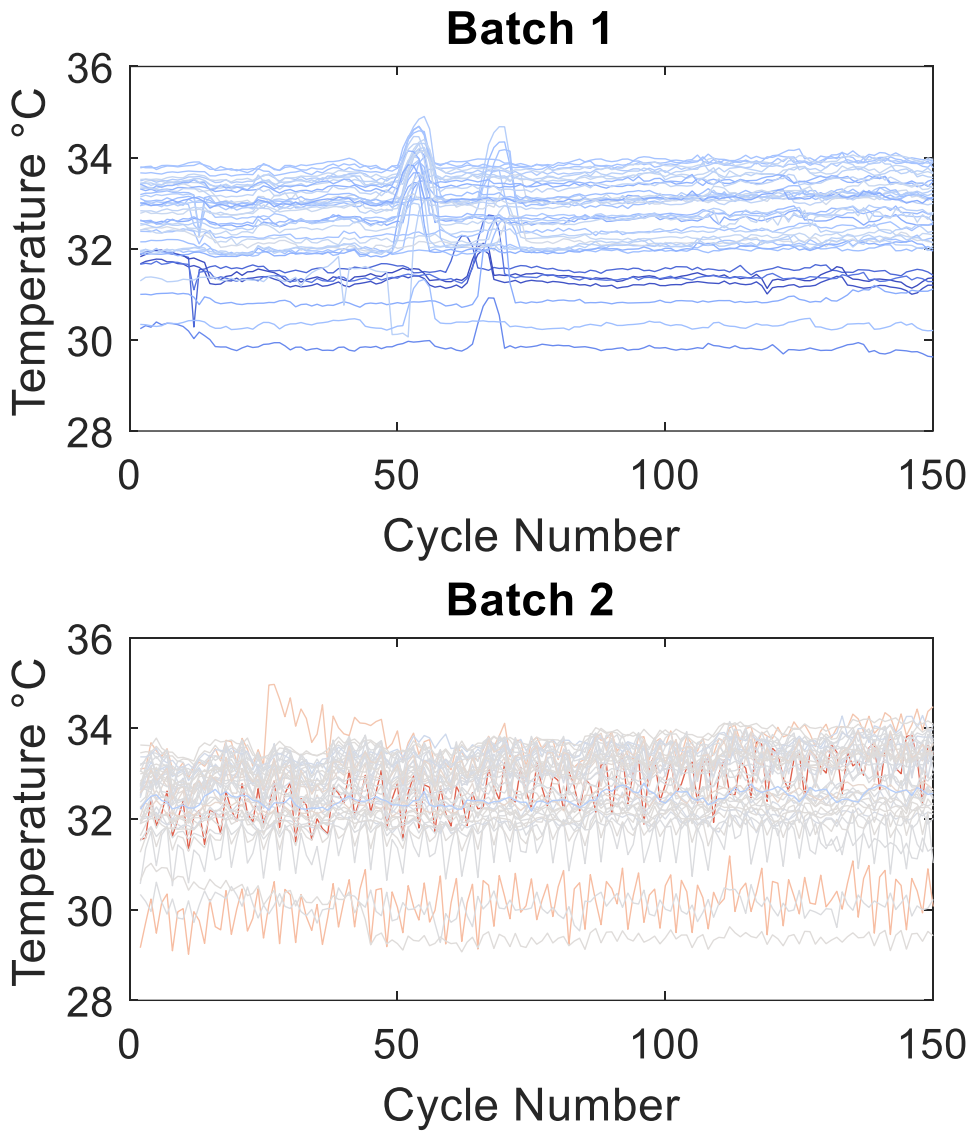
**Supplementary Figure 23.** Results of an alternate indexing scheme for the  $\Delta Q(V)$  features. **a**, The early index is determined based on the maximum achieved capacity index,  $h_i$ , indicated for each battery,  $i$ , by a black **x**. The  $\Delta Q(V)$  is then calculated as  $Q_k(V) - Q_{hi}(V)$  where  $k = j + h_i - \max_i h_i$  such that each  $\Delta Q(V)$  uses the same number of elapsed cycles. **b, c** The average errors for models using the variance of  $\Delta Q(V)$  for the training (**b**) and test (**c**) data.



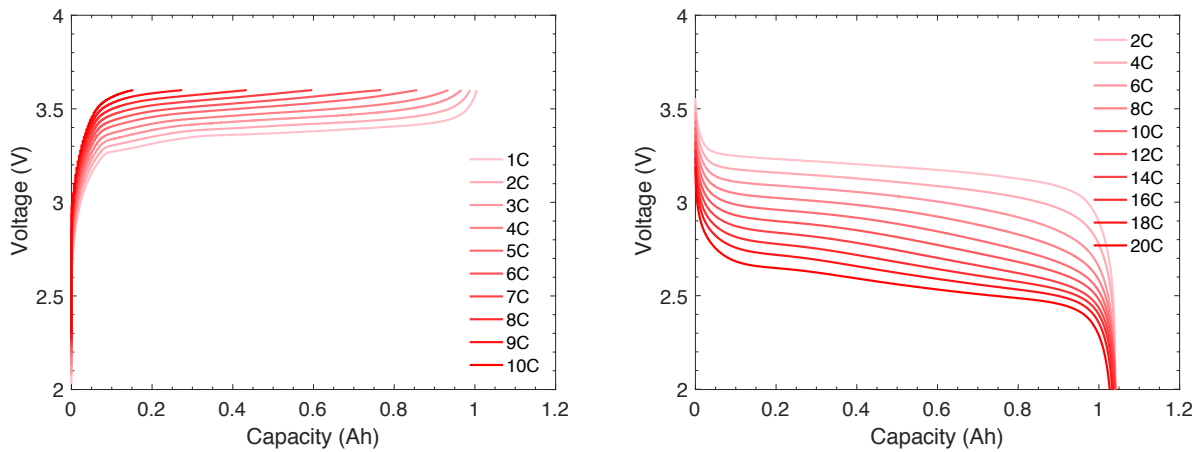
**Supplementary Figure 24.** Example of indices selection for applying the  $\Delta Q(V)$  features using the relative discharge capacity curves. Each discharge capacity is scaled by the maximum discharge capacity value (shown in Supplementary Figure 23a). Each  $\times$  indicates a cycle corresponding to a relative discharge capacity of 0.995.



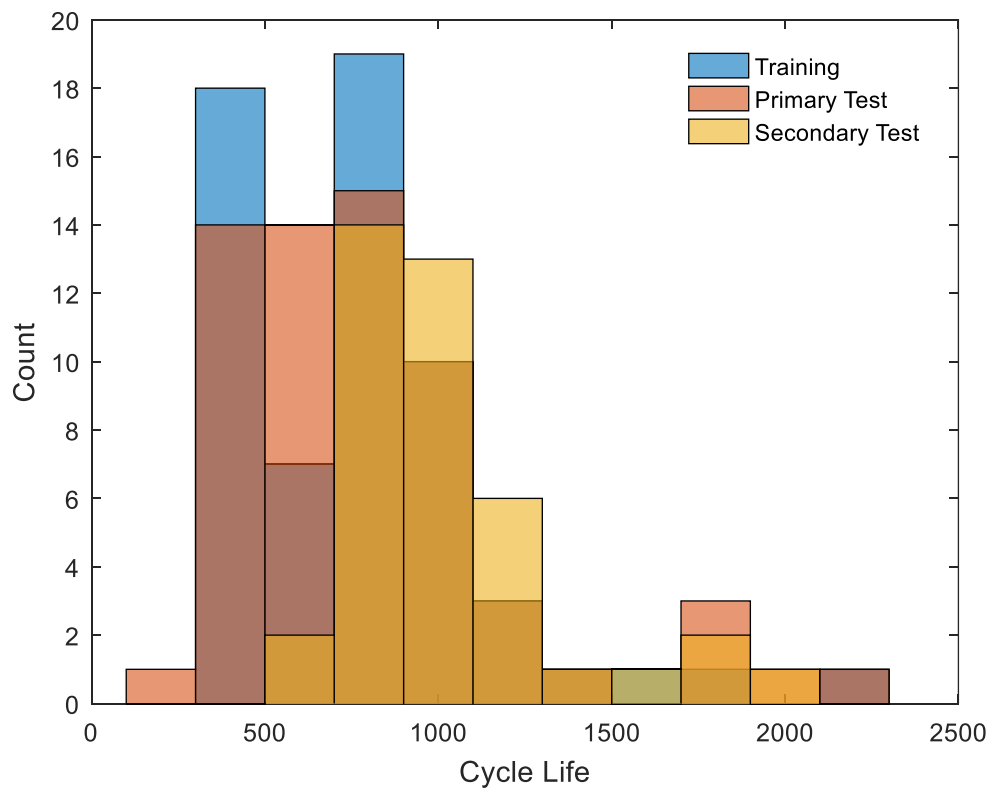
**Supplementary Figure 25.** Results of an alternate indexing scheme for the  $\Delta Q(V)$  features. The indices are based on when the discharge capacity reaches a relative capacity fade. Relative capacity is determined by dividing the discharge capacity trajectory by the maximum capacity achieved by the battery. An example is shown in Supplementary Figure 24. The model uses the variance of  $\Delta Q(V)$ . The upper colorbar limit is set to 400 cycles to improve readability.



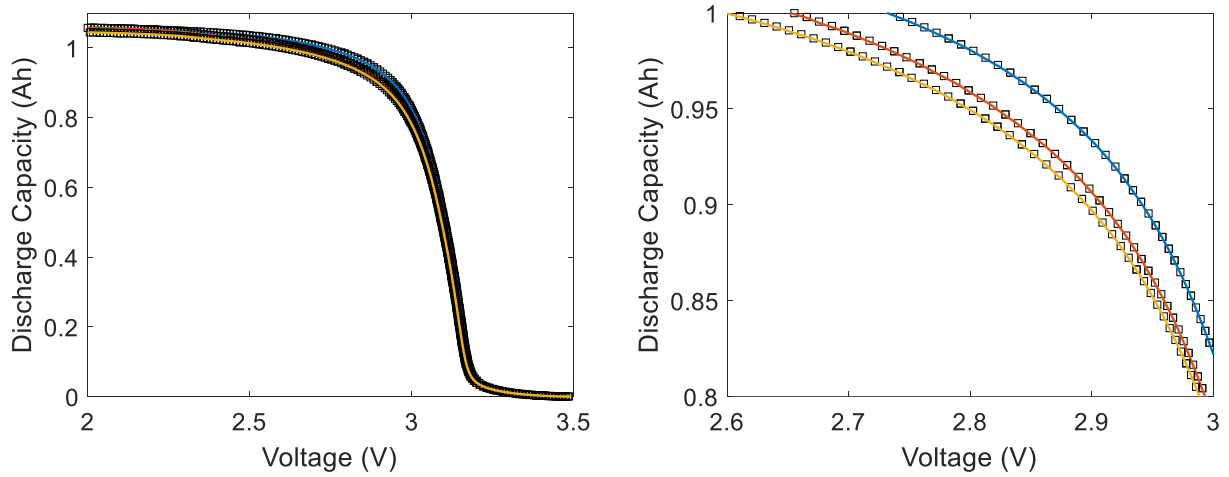
**Supplementary Figure 26.** The average temperature for each of the batteries in “batch1” and “batch2” over the first 150 cycles. The two brief spikes in temperature observed in “batch1” corresponds to the decrease in performance observed in Figure 5. This event impacted approximately 50% of the cells in the test and train datasets and is likely responsible for the high-error (yellow) regions in Figure 5 for  $i=60$  through  $i=70$ . The temperature remained constant during “batch2”, which consisted of the other 50% of the cells in the train and test datasets.



**Supplementary Figure 27.** Rate capability during charge (left) and discharge (right) for a pristine A123 18650 M1A cell. The voltage limits were 3.6 V and 2.0 V. The discharging rate was 1C for the charge test, and the charge rate was 1C for the discharge test. Only the constant-current portion is shown; the constant-voltage portion is not shown.



**Supplementary Figure 28.** Histogram of cycle life for the training, primary test, and secondary test datasets.



**Supplementary Figure 29.** Spline fits (solid lines) to the discharge capacity as a function of voltage (black squares) for three batteries at cycle 100. A smoothing spline accurately captures the relationship between discharge capacity and voltage and enables facile vector manipulation of the data.

## Supplementary Tables

**Supplementary Table 1.** Features considered for the three regression model implementations.

The simplest model (“variance”) uses only the log variance of  $\Delta Q_{100-10}(V)$  and does not consider model selection. The “discharge” model uses only discharge information for feature generation (first two sections), while the “full” model uses charge time, temperature, and internal resistance as additional measurements for feature generation (all sections).

	Features	“Variance”	“Discharge”	“Full”
$\Delta Q_{100-10}(V)$ features	Minimum		✓	✓
	Mean			
	Variance	✓	✓	✓
	Skewness		✓	
	Kurtosis		✓	
	Value at 2V			
Discharge capacity fade curve features	Slope of the linear fit to the capacity fade curve, cycles 2 to 100			✓
	Intercept of the linear fit to capacity fade curve, cycles 2 to 100			✓
	Slope of the linear fit to the capacity fade curve, cycles 91 to 100			
	Intercept of the linear fit to capacity fade curve, cycles 91 to 100			
	Discharge capacity, cycle 2		✓	✓
	Difference between max discharge capacity and cycle 2		✓	
	Discharge capacity, cycle 100			
Other features	Average charge time, first 5 cycles			✓
	Maximum temperature, cycles 2 to 100			
	Minimum temperature, cycles 2 to 100			
	Integral of temperature over time, cycles 2 to 100			✓

	Internal resistance, cycle 2			
	Minimum internal resistance, cycles 2 to 100			✓
	Internal resistance, difference between cycle 100 and cycle 2			✓

**Supplementary Table 2.** The features selected in the “multivariate discharge curve” benchmarking models.

	Features	“Multivariate discharge curve, cycle 100”	“Multivariate discharge curve, cycle 300”
<b>Multivariate discharge curve features</b>	Slope of capacity fade curve, cycles 2 to 100/300	✓	✓
	Intercept of the linear fit to capacity fade curve, cycles 2 to 100/300	✓	✓
	Slope of capacity fade curve, cycles 91 to 100 or 291 to 300	✓	✓
	Intercept of the linear fit to the capacity fade curve, cycles 91 to 100 or 291 to 300		✓
	Discharge capacity, cycle 2	✓	✓
	Max discharge capacity – discharge capacity, cycle 2	✓	✓
	Discharge capacity, cycle 100/300	✓	✓

**Supplementary Table 3.** Model metrics for all benchmarking models. Train and test refer to the data used to learn the model and evaluate model performance, respectively. One battery in the test set reaches 80% SOH rapidly and does not match other observed patterns. Therefore, the parenthetical test results correspond to the exclusion of this battery. This battery is excluded from the “multivariate discharge curve, cycle 300” model since it already reached 80% SOH by cycle 300.

	RMSE (cycles)			Mean Percent Error		
	Train	Primary Test	Secondary Test	Train	Primary Test	Secondary Test
“Constant” model	327	401 (399)	511	29.6%	34.9% (28.2%)	36.1%
“Discharge at cycle 100” model	304	373 (378)	577	25.0%	26.4% (24.7%)	45.3%
“Slope of discharge 91-100” model	307	370 (374)	488	25.1%	26.1% (25.7%)	33.7%
“Multivariate discharge curve, cycle 100” model	243	629 (323)	624	18.8%	78.5% (23.1%)	50.0%
“Multivariate discharge curve, cycle 300” model	167	352	561	12.5%	(26.9%)	45.5%

**Supplementary Table 4.** Confusion matrix for the classification task with the “variance classifier” using a maximum cycle number of 5 and a lifetime threshold of 550. The values in the addition expressions are for train, primary test, and secondary test, respectively. The accuracies are 82.1%, 78.6%, and 97.5% for train, primary test, and secondary test, respectively. There are 39, 41, and 40 cells in the three groups, respectively.

Observed/Predicted	High lifetime	Low lifetime	Total
<b>High lifetime</b>	$15 + 20 + 39 = 74$	$3 + 3 + 0 = 6$	80
<b>Low lifetime</b>	$4 + 5 + 1 = 10$	$16 + 14 + 0 = 30$	40
<b>Total</b>	84	36	120

**Supplementary Table 5.** Selected features in l1-regularized logistic regression in the “full classifier”. Four of eighteen features were selected.

Feature	Weight
Temperature integral	-1.180
Charge time	0.710
$\min(\Delta Q_{5-4}(V))$	-0.522
$\text{var}(\Delta Q_{5-4}(V))$	-0.462

**Supplementary Table 6.** Confusion matrix for the classification task using the “full classifier” using a maximum cycle number of 5 and a lifetime threshold of 550. The values in the addition expressions are for train, primary test, and secondary test, respectively. The accuracies are 97.4%, 92.7%, and 97.5% for train, primary test, and secondary test, respectively. There are 39, 41, and 40 cells in the three groups, respectively.

Observed/Predicted	High lifetime	Low lifetime	Total
<b>High lifetime</b>	$18 + 19 + 39 = 77$	$0 + 3 + 0 = 3$	80
<b>Low lifetime</b>	$1 + 0 + 1 = 2$	$19 + 19 + 0 = 38$	40
<b>Total</b>	79	41	120

**Supplementary Table 7.** Comparison of the change in discharge energy between cycle ~100 and the beginning of life (cycle 1 or 10) for slow (C/10) diagnostic cycling and fast (4C) standard cycling.

Charging rate	Slow cycling: Cycle 100 – cycle 1 (Wh)	Fast cycling: Cycle 101 – cycle 10 (Wh)	Slow cycling/Fast cycling (%)
4C	-0.0247	0.0182	-136%
6C	0.0357	0.0678	52.7%
8C	0.0841	0.1269	66.3%

**Supplementary Table 8.** Comparison of the change in discharge energy between the end of life and the beginning of life (cycle 1 or 10) for slow (C/10) diagnostic cycling and fast (4C) standard cycling.

Charging rate	Slow cycling: Final cycle – cycle 1 (Wh)	Fast cycling: 2 <sup>nd</sup> -to-last cycle – cycle 10 (Wh)	Slow cycling/Fast cycling (%)
4C	0.2312	0.2811	82.2%
6C	0.2226	0.3838	58.0%
8C	0.2410	0.4042	59.6%

**Supplementary Table 9.** Description of all cells included in dataset. ‘Batch date’ refers to the date the batch started. ‘Charging policy’ refers to the currents between 0% and 80% and are formatted as “C1(Q1%)-C2”, where C1 and C2 represent the first and second applied C rates, respectively, and Q1 represents the SOC at which the current switches (see Supplementary Figure 2). Further details are available at the data repository.

Cell barcode	Dataset	Batch date	Cycle life	Charging policy
EL150800460514	Prim. Test	2017-05-12	1852	3.6C(80%)-3.6C
EL150800460486	Train	2017-05-12	2160	3.6C(80%)-3.6C
EL150800460623	Prim. Test	2017-05-12	2237	3.6C(80%)-3.6C
EL150800464977	Train	2017-05-12	1434	4C(80%)-4C
EL150800464865	Prim. Test	2017-05-12	1709	4C(80%)-4C
EL150800464883	Train	2017-05-12	1074	4.4C(80%)-4.4C
EL150800463886	Prim. Test	2017-05-12	636	4.8C(80%)-4.8C
EL150800465027	Train	2017-05-12	870	4.8C(80%)-4.8C
EL150800460468	Prim. Test	2017-05-12	1054	5.4C(40%)-3.6C
EL150800463882	Train	2017-05-12	788	5.4C(40%)-3.6C
EL150800463838	Prim. Test	2017-05-12	880	5.4C(50%)-3C
EL150800453113	Train	2017-05-12	719	5.4C(50%)-3C
EL150800460653	Prim. Test	2017-05-12	862	5.4C(50%)-3.6C
EL150800460522	Train	2017-05-12	857	5.4C(50%)-3.6C
EL150800453240	Prim. Test	2017-05-12	691	5.4C(60%)-3C
EL150800464881	Train	2017-05-12	788	5.4C(60%)-3C
EL150800464002	Prim. Test	2017-05-12	534	5.4C(60%)-3.6C
EL150800463871	Train	2017-05-12	559	5.4C(60%)-3.6C
EL150800460477	Prim. Test	2017-05-12	1014	5.4C(70%)-3C
EL150800460630	Train	2017-05-12	1017	5.4C(70%)-3C
EL150800460617	Prim. Test	2017-05-12	854	5.4C(80%)-5.4C
EL150800460659	Train	2017-05-12	870	5.4C(80%)-5.4C
EL150800463198	Prim. Test	2017-05-12	842	6C(30%)-3.6C
EL150800460507	Train	2017-05-12	860	6C(30%)-3.6C
EL150800460644	Prim. Test	2017-05-12	917	6C(40%)-3C
EL150800460615	Train	2017-05-12	709	6C(40%)-3C
EL150800460481	Prim. Test	2017-05-12	876	6C(40%)-3.6C
EL150800460640	Train	2017-05-12	731	6C(40%)-3.6C
EL150800460436	Prim. Test	2017-05-12	757	6C(50%)-3C
EL150800460525	Train	2017-05-12	742	6C(50%)-3C
EL150800460622	Prim. Test	2017-05-12	703	6C(50%)-3.6C
EL150800460506	Train	2017-05-12	704	6C(50%)-3.6C
EL150800460601	Prim. Test	2017-05-12	648	6C(60%)-3C
EL150800453773	Train	2017-05-12	617	6C(60%)-3C

EL150800460642	Prim. Test	2017-05-12	625	7C(30%)-3.6C
EL150800463229	Train	2017-05-12	966	7C(30%)-3.6C
EL150800460647	Prim. Test	2017-05-12	1051	7C(40%)-3C
EL150800460618	Train	2017-05-12	702	7C(40%)-3C
EL150800460636	Prim. Test	2017-05-12	651	7C(40%)-3.6C
EL150800460485	Train	2017-05-12	616	7C(40%)-3.6C
EL150800460656	Prim. Test	2017-05-12	599	8C(15%)-3.6C
EL150800460518	Train	2017-06-30	300	1C(4%)-6C
EL150800460605	Prim. Test	2017-06-30	148	2C(10%)-6C
EL150800460602	Train	2017-06-30	438	2C(2%)-5C
EL150800460673	Prim. Test	2017-06-30	335	2C(7%)-5.5C
EL150800460655	Train	2017-06-30	444	3.6C(22%)-5.5C
EL150800460635	Prim. Test	2017-06-30	480	3.6C(2%)-4.85C
EL150800460634	Train	2017-06-30	511	3.6C(30%)-6C
EL150800460451	Prim. Test	2017-06-30	561	3.6C(9%)-5C
EL150800460466	Train	2017-06-30	477	4C(13%)-5C
EL150800460510	Prim. Test	2017-06-30	458	4C(31%)-5C
EL150800463208	Train	2017-06-30	483	4C(40%)-6C
EL150800460449	Prim. Test	2017-06-30	485	4C(4%)-4.85C
EL150800460478	Train	2017-06-30	494	4.4C(24%)-5C
EL150800460480	Prim. Test	2017-06-30	487	4.4C(47%)-5.5C
EL150800440551	Train	2017-06-30	461	4.4C(55%)-6C
EL150800460652	Prim. Test	2017-06-30	502	4.4C(8%)-4.85C
EL150800460603	Train	2017-06-30	489	4.65C(19%)-4.85C
EL150800463245	Prim. Test	2017-06-30	513	4.65C(44%)-5C
EL150800460501	Train	2017-06-30	527	4.65C(69%)-6C
EL150800460597	Prim. Test	2017-06-30	495	4.8C(80%)-4.8C
EL150800460611	Train	2017-06-30	461	4.8C(80%)-4.8C
EL150800460596	Prim. Test	2017-06-30	471	4.8C(80%)-4.8C
EL150800460614	Train	2017-06-30	468	4.9C(27%)-4.75C
EL150800460610	Prim. Test	2017-06-30	509	4.9C(61%)-4.5C
EL150800460604	Train	2017-06-30	498	4.9C(69%)-4.25C
EL150800460527	Prim. Test	2017-06-30	481	5.2C(10%)-4.75C
EL150800460608	Train	2017-06-30	492	5.2C(37%)-4.5C
EL150800460631	Prim. Test	2017-06-30	519	5.2C(50%)-4.25C
EL150800460641	Train	2017-06-30	520	5.2C(58%)-4C
EL150800460492	Prim. Test	2017-06-30	499	5.2C(66%)-3.5C
EL150800460628	Train	2017-06-30	463	5.2C(71%)-3C
EL150800460528	Prim. Test	2017-06-30	535	5.6C(25%)-4.5C
EL150800460511	Train	2017-06-30	478	5.6C(38%)-4.25C
EL150800460649	Prim. Test	2017-06-30	465	5.6C(47%)-4C
EL150800460627	Train	2017-06-30	459	5.6C(58%)-3.5C
EL150800460526	Prim. Test	2017-06-30	499	5.6C(5%)-4.75C
EL150800460513	Train	2017-06-30	429	5.6C(65%)-3C
EL150800460473	Prim. Test	2017-06-30	466	6C(20%)-4.5C

EL150800460498	Train	2017-06-30	462	6C(31%)-4.25C
EL150800460474	Prim. Test	2017-06-30	457	6C(40%)-4C
EL150800460613	Train	2017-06-30	487	6C(4%)-4.75C
EL150800460678	Prim. Test	2017-06-30	429	6C(52%)-3.5C
EL150800460599	Prim. Test	2017-06-30	713	6C(60%)-3C
EL150800737329	Sec. test	2018-04-12	1009	5C(67%)-4C
EL150800737313	Sec. test	2018-04-12	1063	5.3C(54%)-4C
EL150800737280	Sec. test	2018-04-12	1115	5.6C(36%)-4.3C
EL150800739476	Sec. test	2018-04-12	1048	5.6C(19%)-4.6C
EL150800737213	Sec. test	2018-04-12	828	5.6C(36%)-4.3C
EL150800737229	Sec. test	2018-04-12	667	3.7C(31%)-5.9C
EL150800737307	Sec. test	2018-04-12	1836	4.36C(80%)-4.36C
EL150800737233	Sec. test	2018-04-12	828	5C(67%)-4C
EL150800737270	Sec. test	2018-04-12	1039	5.3C(54%)-4C
EL150800737277	Sec. test	2018-04-12	1078	4.36C(80%)-4.36C
EL150800737276	Sec. test	2018-04-12	817	5.6C(19%)-4.6C
EL150800737314	Sec. test	2018-04-12	932	5.6C(36%)-4.3C
EL150800737319	Sec. test	2018-04-12	816	5.6C(19%)-4.6C
EL150800737387	Sec. test	2018-04-12	858	5.6C(36%)-4.3C
EL150800737386	Sec. test	2018-04-12	876	5.9C(15%)-4.6C
EL150800737345	Sec. test	2018-04-12	1638	4.36C(80%)-4.36C
EL150800737378	Sec. test	2018-04-12	1315	5.3C(54%)-4C
EL150800737274	Sec. test	2018-04-12	1146	5.6C(19%)-4.6C
EL150800737275	Sec. test	2018-04-12	1155	5.6C(36%)-4.3C
EL150800737315	Sec. test	2018-04-12	813	5C(67%)-4C
EL150800737366	Sec. test	2018-04-12	772	3.7C(31%)-5.9C
EL150800737285	Sec. test	2018-04-12	1002	5.9C(60%)-3.1C
EL150800737368	Sec. test	2018-04-12	825	5C(67%)-4C
EL150800737259	Sec. test	2018-04-12	989	5.3C(54%)-4C
EL150800737287	Sec. test	2018-04-12	1028	5.6C(19%)-4.6C
EL150800737251	Sec. test	2018-04-12	850	5.6C(36%)-4.3C
EL150800737234	Sec. test	2018-04-12	541	3.7C(31%)-5.9C
EL150800737320	Sec. test	2018-04-12	858	5.9C(15%)-4.6C
EL150800737380	Sec. test	2018-04-12	935	5.3C(54%)-4C
EL150800737279	Sec. test	2018-04-12	731	5.9C(60%)-3.1C
EL150800737304	Sec. test	2018-04-12	1284	5C(67%)-4C
EL150800737350	Sec. test	2018-04-12	1158	5.3C(54%)-4C
EL150800739477	Sec. test	2018-04-12	1093	5.6C(19%)-4.6C
EL150800737365	Sec. test	2018-04-12	923	5.6C(36%)-4.3C
EL150800737334	Sec. test	2018-04-12	1935	5C(67%)-4C
EL150800737361	Sec. test	2018-04-12	1156	5.3C(54%)-4C
EL150800737390	Sec. test	2018-04-12	796	5.6C(19%)-4.6C
EL150800739495	Sec. test	2018-04-12	786	5.6C(36%)-4.3C
EL150800737369	Sec. test	2018-04-12	940	5.3C(54%)-4C
EL150800739484	Sec. test	2018-04-12	1801	4.36C(80%)-4.36C

## Supplementary Note 1. Feature formulations

The formulas for each of the features are given below, ordered as in Supplementary Table 1, moving from top to bottom (unless otherwise noted, log implies log base 10). These features are functions of

$$\Delta Q(V) = Q_{100}(V) - Q_{10}(V), \Delta Q(V) \in \mathbb{R}^p \quad (1)$$

$$\overline{\Delta Q}(V) = \frac{1}{p} \sum_{i=1}^p \Delta Q(V) \quad (2)$$

$$\mathbf{b}^* = \arg \min_{\mathbf{b}} \frac{1}{d} \|\mathbf{q} - \mathbf{X}\mathbf{b}\|_2^2, \quad (3)$$

where  $d$  is the number of cycles used in the prediction,  $\mathbf{q} \in \mathbb{R}^d$  is a vector of discharge capacities as a function of the cycle number,  $\mathbf{X} \in \mathbb{R}^{d \times 2}$  where the first column are the cycle numbers used in prediction and the second column is ones, and  $\mathbf{b} \in \mathbb{R}^2$  is a coefficient vector. The features are

- Minimum =  $\log(|\min(\Delta Q(V))|)$
- Mean =  $\log(|\overline{\Delta Q}(V)|)$
- Variance =  $\log \left( \left| \frac{1}{p-1} \sum_{i=1}^p (\Delta Q(V) - \overline{\Delta Q}(V))^2 \right| \right)$
- Skewness =  $\log \left[ \left| \frac{\frac{1}{p} \sum_{i=1}^p (\Delta Q(V) - \overline{\Delta Q}(V))^3}{\left( \sqrt{\sum_{i=1}^p (\Delta Q(V) - \overline{\Delta Q}(V))^2} \right)^3} \right| \right]$
- Kurtosis =  $\log \left[ \left| \frac{\frac{1}{p} \sum_{i=1}^p (\Delta Q(V) - \overline{\Delta Q}(V))^4}{\left( \frac{1}{p} \sum_{i=1}^p (\Delta Q(V) - \overline{\Delta Q}(V))^2 \right)^2} \right| \right]$
- Value at 2 V =  $\log(|\Delta Q(V = 2)|)$
- Slope of discharge curve, cycles 2 to 100 = the first value in the vector  $\mathbf{b}^*$  as in eqn. 3

where  $d = 99$

- Intercept of the linear fit to  $Q(n)$ , cycles 2 to 100, the second value in the vector  $\mathbf{b}^*$  as in eqn. 3 where  $d = 99$
- Slope of  $Q(n)$ , cycles 91 to 100 = the first value in the vector  $\mathbf{b}^*$  as in eqn. 3 where  $d = 10$
- Intercept of the linear fit to  $Q(n)$ , cycles 91 to 100, the second value in the vector  $\mathbf{b}^*$  as in eqn. 3 where  $d = 10$
- Discharge capacity, cycle 2 =  $Q(n = 2)$
- Max discharge capacity – discharge capacity, cycle 2 =  $\max_n Q(n) - Q(n = 2)$
- Discharge capacity, cycle 100 =  $Q(n = 100)$
- Average charge time =  $\frac{1}{5} \sum_{i=2}^6 \text{Charge Time}_i$
- Maximum temperature, cycles 2 to 100 =  $\max_n T(n)$
- Minimum temperature, cycle 2 to 100 =  $\min_n T(n)$
- Temperature integral, cycle 2 to 100 =  $\int_{t_2}^{t_{100}} T(t) dt$
- Internal resistance, cycle 2 =  $IR(n = 2)$
- Minimum internal resistance =  $\min_n IR(n)$
- Internal resistance, cycle 100 – cycle 2 =  $IR(n = 100) - IR(n = 2)$

We note that  $\Delta Q(V)$  can be related to the change in energy of the battery over cycles. For a battery cycled galvanostatically between  $V_1$  and  $V_2$ , the energy is given by

$$E = \int_{V_1}^{V_2} Q(V) dV \quad (4)$$

A change in energy,  $\Delta E$ , is given by

$$\Delta E = \int_{V_1}^{V_2} Q_{100}(V) dV - \int_{V_1}^{V_2} Q_{10}(V) dV = \int_{V_1}^{V_2} (Q_{100}(V) - Q_{10}(V)) dV \quad (5)$$

Various transformations of  $\Delta Q(V)$  are correlated with a change in energy.

## **Supplementary Note 2. Secondary test set error**

From Table 1, the error for the discharge model applied to the secondary test set is 8.6%, while the error for the full model applied to the secondary test set is 10.7%. While the differences are small, this result is counterintuitive given the additional features and data streams provided. We believe two factors can explain this counterintuitive result.

First, the sample size is small. We expect that, with additional samples, we would be able to show that additional measurement streams (e.g. temperature and internal resistance) contributing to the feature set would lead to improved performance.

Second, the calendar aging of the secondary test set was about one year greater than the primary testing and training sets. Calendar aging impacts the initial capacity of the cell (Supplementary Figure 6). This change introduces bias for the secondary test dataset for the features based on the discharge capacity fade curve.

While we expect to see this bias in both the discharge and full models, our analysis indicates that this effect manifests more strongly in the discharge model given the specific features selected in the discharge and full models. Supplementary Figure 7 shows the contribution of all discharge features (weight times value) relative to the average cycle life prediction for both the discharge and full models for the secondary test dataset. In the discharge model, these features include (1) the discharge capacity at cycle 2 and (2) the difference between the max discharge capacity and cycle 2. In the full model, these features include (1) the slope of the linear fit to the capacity fade curve, cycles 2 to 100, (2) the intercept of the linear fit to capacity fade curve, cycles 2 to 100, and (3) the discharge capacity at cycle 2.

In both cases, the discharge features decrease the predicted cycle life, but the decrease is much larger in the case of the full model. As a result, the calendar life effect reduces the

predicted lifetime in the full model. A final application of the model could take into account calendar aging to correct for these effects.

### **Supplementary Note 3. Benchmarking models**

Five naïve models were considered for benchmarking:

1. “**Constant**”: univariate model using only the average cycle life of the training set for all predictions
2. “**Discharge at cycle 100**”: univariate model using only the discharge capacity at cycle 100
3. “**Slope of discharge cycles 91-100**”: univariate model using only the slope of the linear fit for discharge capacity, cycles 91-100
4. “**Multivariate discharge curve model, cycle 100**”: multivariate model with feature selection using the features described in Supplementary Table 2 (note that these features are the second section of Supplementary Table 1) using data from the first 100 cycles
5. “**Multivariate discharge curve model, cycle 300**”: multivariate model with feature selection using the features described in Supplementary Table 2 (note that these features are the second section of Supplementary Table 1) using data from the first 300 cycles

In all analyses, the same data partitioning into train, primary test, and secondary test is used. The features selected in the multivariate discharge curve models are displayed in Supplementary Table 2. The multivariate discharge curve models are shown in Supplementary Figure 8 and Supplementary Figure 9, and all errors are reported in Supplementary Table 3. The best performing model is the “slope of discharge 91-100” model; the multivariate models have much higher testing error compared to training error, implying these models are overfit. As a whole, models that only use features from the capacity fade curve do not accurately predict cycle

life, particularly for batteries with long cycle lives. The errors of all benchmarking models are significantly larger than those presented in the main text.

Interestingly, the multivariate discharge curve model using the first 300 cycles performs comparably to the model that uses the first 100 cycles. We rationalize this observation by investigating the correlation between cycle life and the capacity at cycles 100, 200, and 300, as displayed in Supplementary Figure 10. The correlations improve slowly with increased cycle number but also become less linear. We attribute this nonlinearity to the nonlinear nature of the capacity fade curves. Overall, this analysis illustrates the difficulty of relying solely on features from the capacity fade curve, even at increased cycle number.

As an additional benchmarking approach, we also consider using capacity fade metrics as the criteria for prediction (i.e. 5% capacity fade), instead of a fixed cycle index (i.e. cycle 100). We find that at 5% capacity fade (both relative and absolute), a linear trend does develop (see Supplementary Figure 11). However, this trend is late to develop. The average number of cycles to reach 5% capacity fade is 508 and 425 cycles for relative and absolute capacity fade, respectively. The correlation coefficient between cycle life and the log variance of  $\Delta Q_{100-10}(V)$  feature is similar to that between the number of cycles to reach 5% capacity fade (0.98 and 0.94 for relative and absolute capacity fade, respectively). While this analysis suggests that capacity fade features can be used to predict cycle life in certain contexts, waiting until a certain capacity fade is reached also has the undesirable property of scaling with cycle life, meaning cells with long cycle lives require more time until a prediction is made.

We also build single-feature linear models using log cycle life as our single feature. Capacity fade was defined as the relative change from the measured capacity at cycle 2. Using

the same training and testing split as in the manuscript, RMSE is calculated for various capacity fade criteria and plotted in Supplementary Figure 12.

Of course, using a relative indexing scheme means that the number of cycles used in prediction varies for each battery. The distribution of the cycle number used in prediction for Supplementary Figure 12 is shown in Supplementary Figure 13. The errors of the capacity fade models are similar to the models using  $\Delta Q(V)$  features at 2% capacity fade, which requires 425 cycles on average. The last prediction for the data occurs at cycle 895.

#### **Supplementary Note 4. Early-cycle classification**

Two types of classification analysis were performed using two thresholds:

##### “Variance classifier”

The first analysis (“variance classifier”) uses only the log variance of  $\Delta Q(V)$  to classify batteries as “low lifetime” or “high lifetime” to create univariate classification models. The data are evenly split into train and test groups of 42 cells using the same train-test split as before, analogously to Figure 5. Test data are z-scored based on the training data. The area under the receiver operator curve (AUC) is then calculated. AUC is a common metric for classification tasks and is a measure of the area under the true positive rate – false positive rate tradeoff curve. An AUC of 0.5 is equivalent to a random classification, and an AUC of unity is perfect separation. We perform 20 bootstrap samples of train/test splits and average the AUC across these trials. The results are shown in Supplementary Figures 14 and 15 for lifetime thresholds of 550 and 700, respectively.

For early cycles ( $i,j < 10$ ), the performance is highest along the  $i=j+1$  diagonal. This trend is seen for both threshold values. We rationalize this observation by considering temperature fluctuations within the chamber (see Supplementary Figure 26). Given the temperature fluctuations on the scale of five cycles, we hypothesize that consecutive cycles are highly performing in these early-cycle contexts because their temperatures are most similar. This effect is less important for predictions with higher degradation, as the effect of degradation supersedes the effect of temperature fluctuations. This result highlights the importance of stable temperature control for factory-based applications.

Given this result, we first develop a univariate model using only the variance of  $\Delta Q(V) = Q_5(V) - Q_4(V)$ . This model is termed “variance classifier”. We select these indices to restrict the

prediction to only use data from the first five cycles. The coefficient weight of the trained model is -0.433. 16 of 120 points are incorrectly classified, highlighting our high performance even at very early cycles. Accuracy information is also presented in Supplementary Table 4 as a confusion matrix. A confusion matrix is a standard representation of the classification accuracy for each class.

Supplementary Figure 16 presents the probability of the cycle life exceeding 550 cycles (in other words, the probability a battery is in the “high lifetime” class) using the “variance classifier”. In this figure, points within the bottom left and top right quadrants are correctly classified, while points within the bottom right and top left quadrants are incorrectly classified. We select a probability of 0.5 as the decision boundary.

#### “Full classifier”

The second analysis (“full classifier”) investigates multivariate classification models using features from only the first five cycles. We develop a regularized logistic regression model to classify batteries into “low lifetime” and “high lifetime” classes, selecting 550 cycles as the lifetime threshold. In logistic regression, the logit function is employed to estimate probabilities of an event. The values of probability range from 0 to 1. We use the logistic loss criterion with l1-regularization to train the model and perform subset selection simultaneously, similar to the regularized linear model presented previously.

For the “full classifier”, eighteen of the twenty features from the full model (Supplementary Table 1) are candidate features; however, these features are edited to only draw information up to cycle 5. The late-cycle slope and intercept (slope and intercept for a linear fit between cycles 91 and 100) did not have an analogue in this setting, which removed two of the

twenty features. Again, cycles 5 and 4 are used for  $\Delta Q(V)$ . The selected features and their weights are presented in Supplementary Table 5 for a threshold of 550 cycles.

We find that the temperature integral is the most highly weighted feature, in line with our previous rationalization of the importance of temperature in very-early-cycle prediction tasks. Two  $\Delta Q_{5-4}(V)$  features, the minimum and the variance, were selected, further showcasing the predictive power of this feature.

Supplementary Figure 17 presents the probability of the cycle life exceeding 550 cycles (in other words, the probability a battery is in the “high lifetime” class) for the “full classifier”. This Supplementary Figure should be read in a similar manner as Supplementary Figure 16. Again, we select a probability of 0.5 as the decision boundary.

Five of 120 points are incorrectly classified, highlighting our high performance even at very early cycles. This information is also presented in Supplementary Table 6, the confusion matrix.

## Supplementary Note 5. Degradation quantification

Supplementary Figure 19 plots the shifts in both LLI and LAM<sub>deNE</sub> as a function of C rate and cycle number for both the change after 100 cycles and the total lifetime of the cells (based on the shift quantification presented in Supplementary Figure 18). For the first 100 cycles, the shifts in both LLI and LAM<sub>deNE</sub> increase with C rate. At the end of life, the overall shifts are quite similar, indicating that the end states are similar. We note that while LLI is occurring within the first 100 cycles (indicating a decrease in capacity), the overall capacity generally increases by cycle 100 (Figure 1c) due to the “overhang effect” reported by other groups<sup>56-57</sup>.

The trend in the shifts for the first 100 cycles is notable because the shifts increase with increasing C rate, despite a lower time per cycle as the C rate increases. This observation suggests that calendar aging (i.e. time-dependent aging) plays only a small role during fast charging. We propose some hypotheses for these dependences on C rate here:

- Loss of lithium inventory (LLI)
  - **More SEI growth due to increased temperature.** SEI growth rates are known to increase with temperature,<sup>1,2</sup> which would in turn increase with C rate.
  - **More SEI growth due to increased overpotential.** SEI growth rates would increase with increasing overpotential (decreased anode intercalation potential relative to the standard lithium potential).<sup>2,3</sup> The overpotential would, in turn, increase with C rate.
- Loss of active delithiated negative electrode material (LAM<sub>deNE</sub>)
  - **More delamination/fracture due to increasing strain rate.** Graphite particles could lose contact with the electronic network due to mechanical

factors such as delamination and particle fracture, which would be dictated by the strain rate.<sup>4</sup> The strain rate would increase with increasing C rate.

- **More electrolyte dry-out due to increased temperature.** Graphite could lose ionic contact due to electrolyte dry-out,<sup>5,6</sup> which would increase with temperature and thus C rate.

Studying these mechanisms in depth is the subject of future work.

## Supplementary Note 6. Kinetic degradation

We consider the role of kinetic degradation in the  $\Delta Q(V)$  signal by investigating the capacity discharged during the constant-voltage hold at the end of discharge, which is an accessible metric of kinetic degradation. In fact, we observe a continuous increase in this capacity with cycle number (Supplementary Figure 21), which is one indication that the impedance is increasing with time.

Given that the impedance is clearly increasing, we investigate the relative contributions of the  $\Delta Q(V)$  signal. We can distinguish the effects of OCV degradation modes such as LAM from kinetic degradation modes by comparing the changes in energy between slow cycling and fast cycling. The change in discharge energy between representative slow (C/10) cycles and fast (4C) cycles within each of the three charging conditions is displayed in Supplementary Table 7 (comparison between cycle  $\sim 100$  and beginning of life) and Supplementary Table 8 (comparison between end of life and beginning of life). The change in energy during slow discharging is generally 50%-80% of the total change in energy during high-rate discharging. This result indicates that OCV degradation modes contributes significantly to the  $\Delta Q(V)$  signal, but both low-rate and high-rate degradation modes contribute.

Finally, we consider the source of the kinetic contributions to  $\Delta Q(V)$ , which we estimate contributes 20% to 50% of the total impedance. Conventionally, impedance increases are generally attributed to interfacial/interphasial effects such as SEI growth<sup>7,8</sup>; however, we mention that low-rate degradation modes like LAM<sub>deNE</sub> also increase the overpotential by increasing the local current density of the active regions. Contributions to overpotential that increase with additional cycling include:

- Increased impedance for lithium-ion transport due to SEI growth<sup>7,8</sup>; generally scales with  $t^{1/2}$
- Increased heterogeneity of (de)lithiation<sup>9</sup>
- Increased (de)insertion reaction overpotential as LAM occurs (increased local current density); scales logarithmically with a linear change in LAM
- Increased Ohmic overpotential as LAM occurs (increased local current density); scales linearly with a linear change in LAM

Overall, the relative contributions of these modes are difficult to distinguish. Finally, we note that the cell temperatures generally increase with cycling (Supplementary Figure 4), which would decrease the overpotential.

## **Supplementary Note 7. Relative indexing schemes**

Throughout the manuscript,  $\Delta Q(V)$  is defined based on fixed indices, e.g.  $\Delta Q(V) = Q_{100}(V) - Q_{10}(V)$ , irrespective of battery performance. Additional analysis was performed to compare this fixed indexing scheme to relative indexing schemes. In the relative indexing paradigm, indices are chosen based on the relative capacity decrease. There are three primary choices for the baseline capacity: (1) the nominal capacity of the cell reported by the manufacturer, (2) the initial capacity of the cell, or (3) the maximum capacity of the cell. The nominal capacity of the cells used in analysis is 1.1 Ah. Many cells never achieved this capacity, suggesting it is a less useful baseline. Most of the cells experience an initial increase in capacity, which, if used for scaling, shifts the cycle at which the first decrease is observed. This leaves the maximum as the best option for a capacity benchmark.

Two possible indexing schemes using the capacity scaled by its maximum value were investigated. In the first scheme, a fixed number of cycles after the maximum was used. The results of this procedure are shown in Supplementary Figure 23. The errors of the resulting models do decrease in a similar pattern to Figure 5; however, the improvements in predictive power take longer to develop and do not go as low as observed in the fixed indexing scheme.

The second indexing scheme considers choosing each of the indices based on when a particular relative capacity fade is achieved. Supplementary Figure 24 shows an example of the scaled capacity curves as well as the selection of the cycle corresponding to a relative capacity of 0.995. For all cells in the dataset, more than 250 cycles have passed before 99.5% capacity fade is reached. Therefore, this type of indexing scheme clearly delays when predictions can be made. The errors for the resulting models are shown in Supplementary Figure 25. The colorbar is set to match Figure 5. A comparison of these two figures shows that the relative indexing scheme

models have higher error than the fixed indexing scheme models. While this result may initially seem surprising, we suspect that the relative indexing scheme has the effect of collapsing the trend that differentiates the cells by rescaling.

## Supplementary References

1. Smith, A. J., Burns, J. C., Zhao, X., Xiong, D. & Dahn, J. R. A High Precision Coulometry Study of the SEI Growth in Li/Graphite Cells. *J. Electrochem. Soc.* **158**, A447 (2011).
2. Keil, P. *et al.* Calendar Aging of Lithium-Ion Batteries: I. Impact of the Graphite Anode on Capacity Fade. *J. Electrochem. Soc.* **163**, A1872–A1880 (2016).
3. Xia, J., Nie, M., Ma, L. & Dahn, J. R. Variation of coulombic efficiency versus upper cutoff potential of Li-ion cells tested with aggressive protocols. *J. Power Sources* **306**, 233–240 (2016).
4. Vetter, J. *et al.* Ageing mechanisms in lithium-ion batteries. *J. Power Sources* **147**, 269–281 (2005).
5. Mao, Z., Farkhondeh, M., Pritzker, M., Fowler, M. & Chen, Z. Calendar Aging and Gas Generation in Commercial Graphite/NMC-LMO Lithium-Ion Pouch Cell. *J. Electrochem. Soc.* **164**, A3469–A3483 (2017).
6. Kupper, C., Weißhar, B., Rißmann, S. & Bessler, W. G. End-of-Life Prediction of a Lithium-Ion Battery Cell Based on Mechanistic Aging Models of the Graphite Electrode. *J. Electrochem. Soc.* **165**, A3468–A3480 (2018).
7. Zhang, S., Ding, M. S., Xu, K., Allen, J. & Jow, T. R. Understanding Solid Electrolyte Interface Film Formation on Graphite Electrodes. *Electrochim. Solid-State Lett.* **4**, A206 (2001).
8. Zhang, S. S., Xu, K. & Jow, T. R. EIS study on the formation of solid electrolyte interface in Li-ion battery. *Electrochimica Acta* **51**, 1636–1640 (2006).
9. Lewerenz, M., Marongiu, A., Warnecke, A. & Sauer, D. U. Differential voltage analysis as a tool for analyzing inhomogeneous aging: A case study for LiFePO<sub>4</sub>|graphite cylindrical cells. *J. Power Sources* **368**, 57–67 (2017).

